GEOPHYSICAL OBSERVATORY REPORTS

OF THE INSTITUTE OF EARTH PHYSICS
AND SPACE SCIENCE

YEAR

2020

SZÉCHENYI ISTVÁN GEOPHYSICAL OBSERVATORY
SOPRON
2021

GEOPHYSICAL OBSERVATORY REPORTS

OF THE INSTITUTE OF EARTH PHYSICS AND SPACE SCIENCE

YEAR

2020

SZÉCHENYI ISTVÁN GEOPHYSICAL OBSERVATORY

IAGA CODE: NCK

Editors

T. Bozóki, A. Buzás, K. Szabóné André

Contributors/Authors

T. Bozóki	J. Bór	A. Buzás	L. Döbrentei
T. Hegedüs	Z. Jäger	Á. Kis	L. Kuslits
I. Lemperger	Cs. Molnár	T. Molnár	A. Novák
D. Piri	G. Sátori	Cs. Szabó	K. Szabóné André
S. M. Szalai	J. Szendrői	V. Wesztergom	Z. Zelkó

SOPRON

2021

Contents

Preface

The Széchenyi István Geophysical Observatory was founded during the International Geophysical Year (in 1957-58) as a dedicated research infrastructure of the electromagnetic (EM) phenomena of the solid Earth, upper atmosphere and near-Earth space. The observatory is situated on the southern shore of lake Fertő on thick conductive sediment within the Fertő-Hanság National Park. The favorable situation shelters the observatory from most of the anthropogenic EM noises.

Nowadays the spreading common use of space technologies and the increasing exposure of the surface critical infrastructures requires the continuous observation of the state and processes of the Earth's plasma environment which became known as space weather. These, sometimes extreme changes are associated with solar activity. In addition, comprehensive observational data from several solar cycles provide an opportunity to study long-term changes in the energy coupling between the Sun and the planet.

The infrastructure consists of telluric, geomagnetic, atmospheric electricity and broadband EM field measurement systems, lightning detection, ionospheric sounding and additional background measurements like meteorological observation and ground-based support of satellite Earth observation.

The uniquely long geomagnetic and telluric recordings allow us to model and reconstruct the geodinamo and the external source current systems in the ionized upper atmosphere. Furthermore, the contemporary magnetic and electric measurements serve as remote reference for the magnetotelluric deep sounding geophysical exploration method.

Records related to atmospheric electricity and lightning activity enable the investigation of the variations of regional and global thunderstorm activity which are indicators of climate change. Signals from individual lightning strokes can be used to diagnose the momentary state of the plasmasphere.

The observatory is a member of INTERMAGNET, a global network of the geomagnetic observatories. High time resolution (1 Hz) geomagnetic data are uploaded quasi-real time and also displayed real time on the website of the observatory. The DPS-4D digisonde automatically transfers data to the Global Ionospheric Radio Observatory (GIRO) system collecting ionosonde measurements from around the globe. These data are used to study the electron density changes and the plasma motion of the ionosphere in regional and global scales.

A station of the LINET lightning detection network is working in the observatory and contributes to the mapping of lightning strokes in Europe real-time. Data collected by the atmospheric electricity measurement systems are displayed quasi-real time on the website of the observatory. The observatory is part of the Automatic Whistler Detection and Analyzer Network (AWDANet) providing a cheap and effective way to routinely infer the cold plasma distribution of the inner magnetosphere.

Investigating the impact of cutting down nearby trees on measured values of the atmospheric electric potential gradient data

Attila Buzás[1,2*] and József Bór[1]

[1]Institute of Earth Physics and Space Science (ELKH EPSS), Sopron, Hungary

[2]Doctoral School of Earth Sciences, Faculty of Science, Eötvös Loránd University, Budapest, Hungary

Abstract

A group of trees located at the eastern side of the atmospheric electric potential gradient (PG) measurement site in the Széchenyi István Geophysical Observatory at Nagycenk (NCK) was cut down on the 24th February in 2020. In order to assess the impact of this event on the PG measurements, an electrostatic numerical model was built to model the effect of the removal of trees. Moreover, the PG data recorded between 2017 and 2021 were analyzed. It was found that the PG increased by up to 52% after the trees in question were cut down. Based on the numerical model calculations this enhancement was expected to be larger, 78%. Further investigations concerning the seasonal variation of the PG recorded in 2017–2021 affirm that this increase is not part of the regular seasonal variation of the PG and it is an anomaly most likely caused by the diminished electrostatic shielding effect due to the fewer remaining trees.

Keywords: atmospheric electricity, atmospheric electric potential gradient, electrostatic shielding effect, trees, atmosphere–biosphere coupling, numerical modeling, electrostatics.

Introduction

The atmospheric electric potential gradient (PG) is the negative of the vertical component of the atmospheric electric field measured in Vm^{-1} units. It is a widely monitored parameter, usually measured near the ground (ca. at a height of 1–3 m) in geophysical and meteorological observatories all over the globe (Nicoll et al., 2019). The PG is one of the main parameters of the DC part of the so-called atmospheric

*Corresponding author: Attila Buzás (buzas.attila@epss.hu)

Global Electric Circuit (GEC), which is a framework of electric currents connecting the Earth's surface and the lower ionosphere (Rycroft et al., 2012). The PG can be used as a versatile diagnostic tool as it can mirror variations in the GEC, global changes in Earth's climate system, or space weather processes (Rycroft et al., 2012).

PG measurements in the Széchenyi István Geophysical Observatory at Nagycenk, Hungary (NCK) began in 1961 under the supervision of geophysicists Pál Bencze and Ferenc Märcz with a locally developed potential equalizer instrument including radioactive ionizing source (Bencze & Märcz, 1981). Regular maintenance and weekly instrument calibration ensured high data quality over the course of decades up to the present date. In 1998, another locally developed radioactive instrument was installed to measure the PG simultaneously. Ultimately, in 2013, a more state-of-the-art apparatus, a Boltek EFM-100 field mill was deployed (Bór et al., 2020).

The shielding effect of trees

Nearby conducting objects, such as a metallic pole or living trees, bias the equipotential surfaces of the ambient atmospheric electric field, thus they can lower the PG measured in the vicinity (Lees, 1915). This phenomenon is called the electrostatic shielding effect and it contributed greatly to the reported long-term reduction in the PG time series recorded in NCK (Märcz & Harrison, 2003; Williams et al., 2005; Buzás et al., 2021). The site of the PG measurements in NCK is located on a clearing surrounded by groups of trees and a forest. In the course of time, as the trees grew taller, their shielding effect became more and more significant, further lowering the PG near the surface. In order to correct for this unwanted shielding effect, a numerical model based on the finite element method was built. The detailed description of the model can be found in the paper by Buzás et al. (2021).

On the 24th February in 2020, the group of trees that bordered the measuring site at the eastern side was cut down. To quantify the impact of this event, the geometry of the numerical model was changed; the eastern group of trees was removed from the model (Fig. 1). By evaluating the model with the two configurations, the impact of the change in the local geometry on the recorded PG values can be inferred (Fig. 1).

Data and methods

Only the fair-weather PG data of the Boltek EFM-100 field mill (measured at a height of 3 m) that were not corrected for the shielding effect of nearby trees are used in the present study. This study is based on fair-weather PG values which are PG values that were measured in the so-called fair-weather conditions, i.e., in time periods when the effect of local meteorological conditions and clouds is not significant on the PG measurements (Harrison & Nicoll, 2018; Nicoll et al., 2019). As we lack concurrent supplementary meteorological data suitable for identifying fair-weather conditions reliably, fair-weather selection of the PG data was made
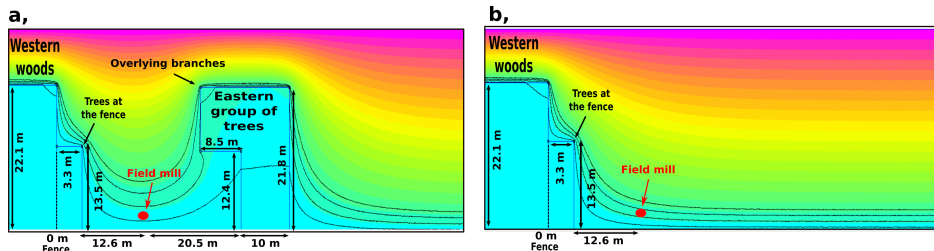
Fig. 1: Model geometry **(a)** before and **(b)** after the eastern trees were cut down on the 24th February, 2020.

on the basis of statistical considerations solely based on the sign and magnitude of the measured PG values. Firstly, negative PG values can be omitted as they are characteristic to foul weather conditions (Harrison & Nicoll, 2018). Moreover, large positive PG values can also be associated with foul weather (e.g., low level charged clouds very near or over the measurement site). Altogether, the positive PG values that were below five times the median of all absolute deviations from the median of the full distribution were considered as fair-weather data (Lucas et al., 2017). Fair-weather correction was made on the original, high time resolution fair-weather PG data recorded at 2 Hz. Hourly averages were calculated from the high time resolution fair-weather data, and these hourly averages were used in all further analysis. In this work, only the fair-weather raw PG data measured at a height of 3 m by the Boltek EFM-100 field mill were used. Note that the data were not corrected either for the shielding effect of nearby trees in any way, or by the form factor of the instrumental setup.

The expected effect of cutting down the trees is estimated using the two numerical models for the site. The modeled PG values are calculated from the two models at the location and height of the EFM-100 measuring head (Fig. 1). The ratio of these two modeled PG values is supposed to mirror the ratio of the measured PG values before and after the change in the configuration of objects onsite.

Since the trees were cut down on a single day, the change in the data, if it appears, should be apparent immediately. Day-to-day variations in the PG, however, can mask smaller differences, so a statistical approach is preferred. Seasonal variation of the PG data (Chalmers, 1967, pp. 168–169), however, imposes a limit on the extension of the time periods of the investigation before and after the tree-cut. To make a compromise, fair weather data from 14 days before and after the tree-cut were considered and the corresponding statistics obtained from the selected measured data were compared.

To investigate how the tree-cut affects the PG measurements in NCK on a longer term, seasonal variation of fair weather data (i.e., monthly averages) were calculated from years of 2017–2021. This way, ratios of the PG data in the same periods of the years before and after the change could be studied.

Results

Derived from calculations based on the two different states of the numerical model before and after the eastern group of trees was cut down, the modeled enhancement of the PG at the location of the Boltek EFM-100 field mill is +78% after the removal of the trees (Fig. 1).

Figure 2 shows the histograms of the PG values recorded two weeks before and after the eastern group of trees was cut out in 2020. The mean, median, and the maximum of the Gaussian Kernel Density Estimation (KDE) function of the PG values taken from the 10–23 Feb 2020 period, two weeks prior to the eastern trees were cut down, are 60 Vm^{-1}, 58 Vm^{-1}, and 57 Vm^{-1}, respectively (Fig. 2a and Tab. I). However, the mean, median, and the maximum of the KDE of the PG values taken from the data recorded two weeks after the trees were cut down (25 Feb–09 Mar 2020) are 89 Vm^{-1}, 88 Vm^{-1}, and 88 Vm^{-1}, respectively (Fig. 2b and Tab. I). This means an enhancement of 29 Vm^{-1} (+48%), 30 Vm^{-1} (+52%), and 31 Vm^{-1} (+54%) when considering the mean, median, and the maximum of the KDE, respectively.
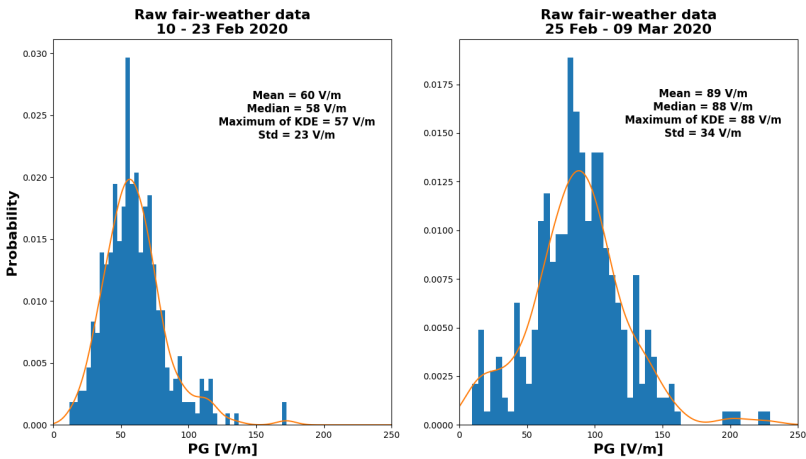
Fig. 2: Histograms of the raw PG data measured two weeks before and after the eastern group of trees was cut down in 2020. Orange solid lines denote the Gaussian Kernel Density estimation functions, an estimation of the probability density function of the raw PG data.

In order to affirm that the enhancement was not caused by the regular seasonal variation of the PG, the mean PG values were calculated for the past three years (2017, 2018, and 2019) and for 2021 in the same time periods (Tab. I). The PG decreased in 2017, 2019, and 2021, or stagnated in 2018 between the time periods

10–23 Feb and 25 Feb–09 Mar, i.e., two weeks before and after the day of the year when the change happened in 2020. Compared to these trends, the PG increased dramatically in the same time period in 2020. This supports the conclusion that the PG increased in 2020 due to the cutting down of the eastern trees, which reduced the shielding effect (Tab. I).

Table I: Mean values of PG data measured 14 days before and after the day of the year (24th February) of cutting the trees. Averages from the years 2017–2021 are given.

	Mean values in years				
	2017	**2018**	**2019**	**2020**	**2021**
PG in 10–23 Feb [V/m]	99	95	79	60	158
PG in 25 Feb–09 Mar [V/m]	73	99	67	89	92
Percental change	-26%	+4%	-15%	**+48%**	-71%

The PG measured at continental stations on the northern hemisphere has a minimum in the summer and reaches its annual maximum during the winter (Chalmers, 1967, pp. 168–169). The PG in the years of 2017, 2018, 2019, and 2021 follows this regular seasonal variation (Fig. 3). However, that is not the case in 2020. In 2020, the PG began to decrease in February, yet it does not continue to diminish in March. In March 2020, there is a significant increase in the PG which is not a regular phenomenon (Fig. 3). This increase was likely caused by the cutting down of the eastern trees on 24th February. Moreover, after February 2020, the PG is higher than the average PG taken from the years 2017–2019 and this continues in 2021 as well (Fig. 3). In 2020 until February, the PG followed the average of the previous years while from March on, the values are clearly closer to the values recorded in the next year. Note that fairly large PG values were measured by the field mill especially in the winter of 2017–2018 in NCK compared to the values recorded in the following years. It is not currently known why those PG values were so large.

The modeled enhancement of the PG values due to the removal of the eastern trees (+78%) overestimates the enhancement that was measured (+48–52%) (Tab. I). In order to examine this difference on a longer time scale, percental differences between the measured monthly PG means in 2017–2021 were calculated (Tab. II). For each month from September to February, the average of the monthly means in the time period 2017–2020 (the first solid red curve in Fig. 3)
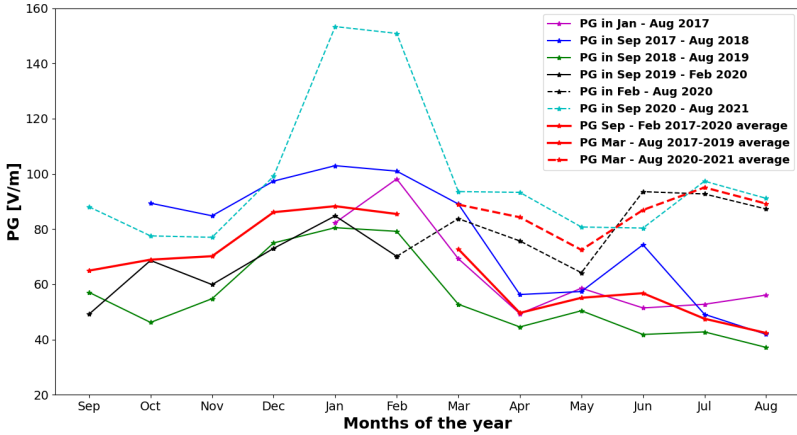
Fig. 3: The seasonal variation of the PG in NCK in years between 2017 and 2021. Note that the years are plotted from September to August to aid comparing measurements before and after the trees were cut down at the end of February, which is now in the middle of the time axis.

Table II: Percental change in averaged monthly PG means after the cutting down of the trees. Data from the years 2017–2021 are considered. See the text for details.

Months	Jan	Feb	Mar	Apr	May	Jun	Jul
Percental difference	+75%	+73%	+26%	+69%	+31%	+56%	+97%
Months	Aug	Sep	Oct	Nov	Dec	**Mean**	
Percental difference	+98%	+66%	+14%	+16%	+21%	**+53%**	

was compared to the monthly mean in 2020–2021 (dashed cyan curve in Fig. 3). For each month from March to August, the average of the monthly means in the time period 2017–2019 (the second solid red curve in Fig. 3) was compared to the average of the monthly means in the time period 2020–2021 (dashed red curve in Fig. 3) (Tab. II). This percental difference is quite variable over the course of months, having higher values during the summer and in January and February, whereas having lower values near the end of the year (Tab. II). The mean of the monthly percental

differences is +53% which is in good accordance with the +48–52% enhancement derived from the PG data two weeks before and after the eastern trees were cut down (Fig. 2; Tab. I and II). Exceptionally high PG values in the January 2017–August 2018 time period enhanced the average taken from 2017–2019 diminish the percental difference between the monthly averages (Fig. 3; Tab. II).

Summary and Conclusions

The group of trees at the eastern side of the PG measurement site in NCK was cut down on 24th February in 2020. This event caused a significant increase in the PG by 48–52% compared to its former value based on the mean PG values taken from the PG data two weeks before and after the cutting down of trees (Fig. 2; Tab. I).

The increase in the PG after the trees were cut out is not a regular enhancement caused by the normal seasonal variation of the PG as the PG decreased in the same periods in 2017, 2019, and 2021 as well (Fig. 3; Tab. I).

The annual variation of the PG in 2020 does not follow the regular annual variation (Fig. 3). The PG in 2020 does not begin to diminish after February. On the contrary, it shows a significant increase from February to March. This phenomenon is most likely caused by the fact that the eastern trees were cut down on the 24th February in 2020.

The numerically modeled increase in the PG is +78% which is higher than the measured one (48–52%). Considering that the PG drops significantly in that period of the year and the generally large variance of the PG values, the agreement between the measured and the modeled change in the PG values is fair. Note that the percental differences between the monthly PG means in 2020–2021 and in 2017–2019 also show a large variability, ranging from +14% (in October) to +98% (in August) (Tab. II). High PG values in January 2017–August 2018 tend to reduce the deduced average percental enhancement causing a larger difference between the modeled and measured enhancements (Fig. 3).

Acknowledgements

References

Bencze, P. & Märcz, F. (1981). The geophysical observatory near Nagycenk II. Atmospheric electric and ionospheric measurements. *Acta Geodaetica, Geophysica et Montanistica Hungarica, 16*, 353–357

Bór, J., Sátori, G., Barta, V., Szabóné-André, K., Szendrői, J., Wesztergom, V., Bozóki, T., Buzás, A., & Koronczay, D. (2020). Measurements of atmospheric electricity in the Széchenyi István Geophysical Observatory. Hungary, *History of Geo- and Space Sciences, 11*, 53–70, https://doi.org/10.5194/hgss-11-53-2020

Buzás, A., Barta, V., Horváth, T., & Bór, J. (2021). Revisiting the long-term decreasing trend of atmospheric electric potential gradient measured at Nagycenk, Hungary, Central Europe. *Annales Geophysicae, 39*, 627–640, https://doi.org/10.5194/angeo-39-627-2021

Chalmers, J. A. (1967). *Atmospheric Electricity* (2nd ed.). United Kingdom, London: Pergamon Press, 515 p.

Harrison, R. G., & Nicoll, K. A. (2018). Fair weather criteria for atmospheric electricity measurements. *Journal of Atmospheric and Solar-Terrestrial Physics, 179*, 239–250, https://doi.org/10.1016/j.jastp.2018.07.008

Lees, C. H. (1915). On the Shapes of Equipotential Surfaces in the Air near Long Walls or Buildings and on their Effect on the Measurement of Atmospheric Potential Gradients. *Proceedings of the Royal Society A, 91*(631), 440–451, https://www.jstor.org/stable/93515

Lucas, G. M., Thayer, J. P., & Deierling, W. (2017). Statistical analysis of spatial and temporal variations in atmospheric electric fields from a regional array of field mills. *Journal of Geophysical Research: Atmospheres, 122*(2), 1158-1174, https://doi.org/10.1002/2016JD025944

Märcz, F., & Harrison, R. G. (2003). Long-term changes in atmospheric electrical parameters observed at Nagycenk (Hungary) and the UK observatories at Eskdalemuir and Kew. *Annales Geophysicae, 21*(11), 2193–2200, https://doi.org/10.5194/angeo-21-2193-2003

Nicoll, K. A., Harrison, R. G., Barta, V., Bór, J., Brugge, R., Chillingarian, A., Chum, J., Georgoulias, A. K., Guha, A., Kourtidis, K., Kubicki, M., Mareev, E., Matthews, J., Mkrtchyan, H., Odzimek, A., Raulin, J.-P., Robert, D., Silva, H. G., Tacza, J., Yair, Y., & Yaniv, R. (2019). A global atmospheric electricity monitoring network for climate and geophysical research. *Journal of Atmospheric and Solar-Terrestrial Physics, 184*, 18–29, https://doi.org/10.1016/j.jastp.2019.01.003

Rycroft, M. J., Nicoll, K. A., Aplin, K. L., & Harrison, R. G. (2012). Recent advances in global electric circuit coupling between the space environment and the troposphere. *Journal of Atmospheric and Solar-Terrestrial Physics, 90–91*, 198–211, https://doi.org/10.1016/j.jastp.2012.03.015

Williams, E., Markson, R., & Heckman, S. (2005). Shielding effects of trees on the measurement of the Earth's electric field: Implications for secular variations of the global electrical circuit. *Geophysical Research Letters, 32*(19), L19810, https://doi.org/10.1029/2005GL023717

ELF Noise Test in the Széchenyi István Geophysical Observatory

Tamás Bozóki[1,2*], József Bór[1], Dániel Piri[1], Attila Novák[1] and Csaba Molnár[1]

[1]Institute of Earth Physics and Space Science (ELKH EPSS), Sopron, Hungary

[2]Doctoral School of Environmental Sciences, University of Szeged, Hungary

Abstract

On the 9th of July, 2020, a detailed noise test was carried out in the Széchenyi István Geophysical Observatory in order to survey the electromagnetic noises generated in the very low frequency (VLF; 3-30 kHz) and extremely low frequency (ELF; 3 Hz - 3 kHz) bands by different electrical devices operating in the observatory. During a ~ 3 hour long period, the measurements of the observatory, the power supply of buildings as well as solar panels and charging of the batteries were shut down one-by-one and finally the main power supply from the nearby village Fertőboz was interrupted for a few minutes. A pair of induction coil magnetometers run from a battery had been installed for this test period and provided information on the changes in the ELF noise environment during the test. Although the ELF-band noise contamination in the measurements reduced in connection to the elimination of internal noise sources in the observatory, it seems that external noise sources outside the observatory are too powerful and prohibit local monitoring of the Schumann resonances in the atmospheric magnetic field. Therefore, a new location for a permanent magnetic SR station is needed.

Keywords: Extremely low frequency, Schumann resonance, ELF noise.

Motivation

Measurements of the atmospheric magnetic field by induction coils in the Széchenyi István Geophysical Observatory (NCK) are contaminated by different artificial noises which hinder the detection of Schumann resonances (SRs) (Sátori et al., 2013; Bór et al., 2020). We usually attribute this noise contamination to the railway lines which run near the observatory and have been electrified well after the establishment of the observatory. In the summer of 2020 a survey of electromagnetic noises was carried out in connection to the re-installation of the renovated VLF antenna. This opportunity enabled us to revisit the question on the origin of ELF noise. The setup of the experiment allowed the separation of ELF noises of internal or external origin in the observatory.

Description of the test measurements

A pair of induction coil magnetometers were installed temporarily near the observatory in the time period from 07/07/2020 to 13/07/2020. The sampling frequency

---

was set to 500 Hz. The measurement ran from a battery which assured the continuous operation throughout the test period. The ~ 3 hour long noise test was carried out on the 9th of July, 2020. It began at 08:45 UT and ended at 11:30 UT. The regular measurements of the observatory, the power supply of buildings as well as solar panels and the batteries they charge were shut down one-by-one during this period. Finally, the main power supply from the nearby village Fertőboz was also interrupted for 6-7 minutes between 11:22 and 11:29 UT.

Results

Figure 1 shows dynamic spectra corresponding to the H_{NS} and H_{EW} field components from the day of the noise test. By comparing them to dynamic spectra corresponding to the very same day but measured in a low ELF noise environment near Magyargencs, Hungary (see Fig. 1 in Bozóki et al., 2021) it is clear that the measurements are highly contaminated by noise. The noise contamination is higher in the H_{NS} field component than in the H_{EW} field component. SRs are faintly visible in the H_{EW} field component, especially before midnight when the noise contamination seems to be the lowest on this day. During the noise test (which took place between 08:45 and 11:30 UT) the diminishment of certain narrowband noises (e.g., at around 30 Hz) can be observed. An intensive, wideband noise (present in both field components) vanished as well around 9:00 UT but it is not clear whether this disappearance had something to do with the noise test because the noise did not appear again after finishing the noise test.

Figure 2 shows a view zoomed in on the test period. The upper limit of the color scale has been modified in this figure to reduce the number of saturated data points. SRs are more clearly visible in the H_{EW} field component during the test period and they faintly appear in the H_{NS} field component as well. However, the noise contamination is still high in both field components. Note that at around 11:30 UT, a narrow stripe with remarkably reduced noise contamination can be seen in the dynamic spectrum of the H_{NS} field component. This time interval seems to coincide with the full shutdown of the observatory's power supply which took place between 11:22 and 11:29 UT. To investigate the ELF noise conditions during this time interval we averaged spectra for 6-min long intervals before (11:16-11:21 UT), during (11:23-11:28 UT) and after (11:30-11:35 UT) the full shutdown (Fig. 3). It is clear that the full shutdown of the observatory's power supply reduced the noise contamination in the H_{NS} field component significantly. However, SRs are still not really visible in the spectrum during this time interval with reduced noise. The remaining noise contamination must come from outside the observatory, probably in connection to the nearby electrified railway line. On the other hand, the noise level in the H_{EW} field component is practically the same in all of the three time intervals which suggest that the internal noise sources in the observatory are direction specific.

We can conclude that even by eliminating all the internal noise sources in the observatory (which is a huge technical challenge that is not solved yet) we cannot obtain clear ELF spectra, therefore a new location is needed for a permanent magnetic ELF station where SRs can be detected in a low ELF noise environment.
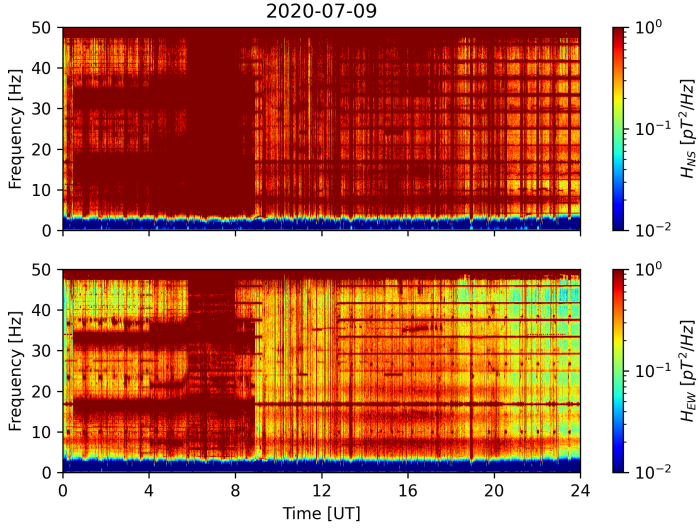
Fig. 1: Dynamic spectra corresponding to the H_{NS} (top panel) and H_{EW} (bottom panel) field components from the day of the noise test which began at 08:45 UT and ended at 11:30 UT.
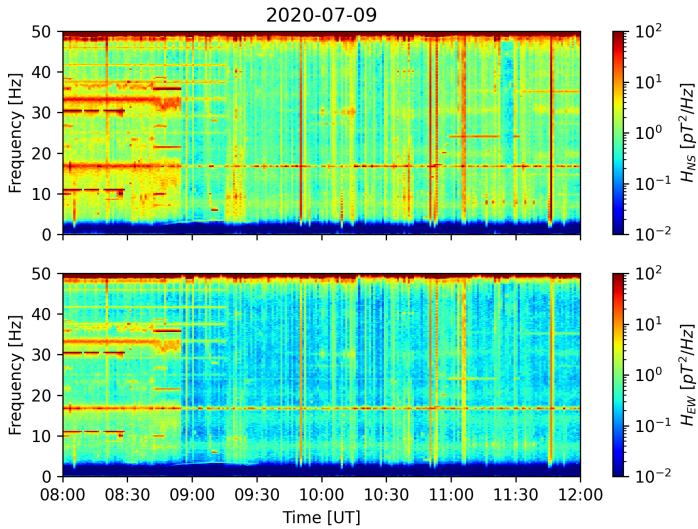

Fig. 2: The same dynamic spectra as in Fig. 1 for the 8:00 - 12:00 UT time period.
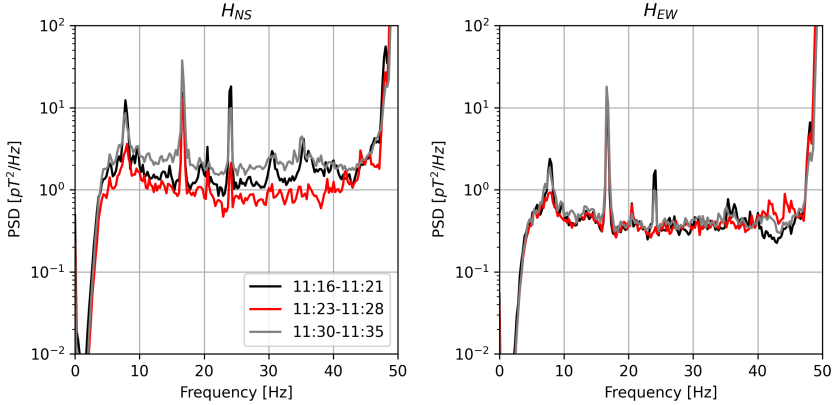
Fig. 3: 6-min average power spectral density (PSD) spectra corresponding to time intervals before (11:16-11:21 UT), during (11:23-11:28 UT) and after (11:30-11:35 UT) the full shutdown of the observatory's power supply on the 9th of July, 2020.

Acknowledgements

References

Bozóki, T., Bór, J., Novák, A., & Molnár, Cs. (2021). ELF field measurements near Magyargencs, Hungary. *Geophysical Observatory Reports* present issue

Bór, J., Sátori, G., Barta, V., Szabóné-André, K., Szendrői, J., Wesztergom, V., Bozóki, T., Buzás, A., & Koronczay, D. (2020). Measurements of atmospheric electricity in the Széchenyi István Geophysical Observatory, Hungary. *History of Geo- and Space Sciences, 11*(1), 53-70, https://doi.org/10.5194/hgss-11-53-2020

Sátori, G., Rycroft, M., Bencze, P., Märcz, F., Bór, J., Barta, V., Nagy, T., & Kovács, K. (2013). An Overview of Thunderstorm-Related Research on the Atmospheric Electric Field, Schumann Resonances, Sprites, and the Ionosphere at Sopron, Hungary. *Surveys in Geophysics, 34*, 255-292, https://doi.org/10.1007/s10712-013-9222-6

ELF field measurements near Hortobágy and Magyargencs

Tamás Bozóki[1,2*], József Bór[1], Attila Novák[1] and Csaba Molnár[1]

[1]Institute of Earth Physics and Space Science (ELKH EPSS), Sopron, Hungary

[2]Doctoral School of Environmental Sciences, University of Szeged, Hungary

Abstract

Extremely low frequency (ELF) field measurements were organized near Hortobágy in 2019 and near Magyargencs in 2020 to survey the observability of Schumann resonances (SR) and properties of the ELF noise environment in the magnetic field in Hungary. The measurements serve our aim to find an appropriate location for a new permanent magnetic SR station. The location of the second test site (near Magyargencs) was selected on the base of experience we gathered from reprocessing high frequency magnetotelluric (MT) measurements in Hungary. Initial evaluation of the field measurements confirmed that it is not easy, but possible to find places of such low ELF noise levels in Hungary, which are suitable for monitoring SR.

Keywords: Extremely low frequency, Schumann resonance, Magnetotellurics.

Motivation

Recording of the magnetic field in the ELF band began in November 1996 in the Széchenyi István Geophysical Observatory (NCK) near Nagycenk, Hungary (Sátori et al., 2013; Bór et al., 2020). Unfortunately, the strong disturbing effect of the nearby electrified railway line hinders the detection of clear ELF spectra and the extraction of high-quality spectral parameters of SRs from these measurements. This strong, artificial noise contamination in the ELF band, which is connected to stray currents induced by the railway traffic, varies in time and in frequency which makes its analog or digital filtering practically impossible. Therefore, our group has decided to find a new location appropriate for establishing a new permanent magnetic SR station. In order to gain a more general knowledge about ELF noise conditions in Hungary and to find the most appropriate location for the planned station, field measurements were organized and high frequency MT measurements (with sampling frequency that enables the observation of SRs) were evaluated.

---

*Corresponding author: Tamás Bozóki (bozoki.tamas@epss.hu)

Description of the measurements

First, two test measurement campaigns were organized near Hortobágy in Eastern Hungary (47.577192° N, 20.940759° E) in 2019. The location was in the area of a large national park, far from railway traffic and industrial areas. The first campaign was about 24 hour long (2-3 October, 2019) while the second, more than two week long campaign took place between the 25th of November and the 12th of December, 2019. Next, high frequency MT measurements made earlier at 8 locations in Hungary were re-processed to survey the suitability of the covered area for making specifically SR observations. Based on the experience we gathered from this analysis, a second test location was selected near the village Magyargencs at the border of the Little Hungarian Plain in western Hungary (47.385014° N and 17.199848° E), closer to NCK. The field measurement near Magyargencs started on the 8th of July and ended on the 30th of July, 2020. All these locations are displayed on Fig. 1.
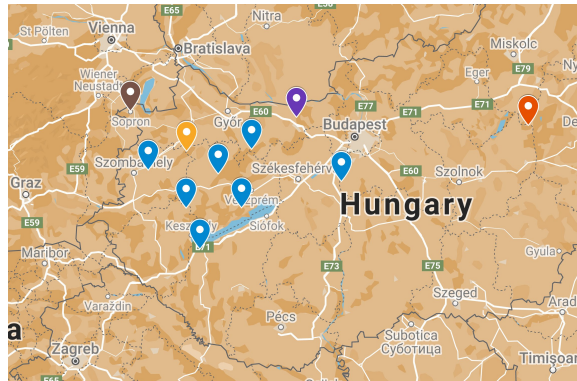

Fig. 1: Location of Sopron (brown), the field measurements (red: Hortobágy, orange: Magyargencs) and the 8 MT sites (7 stations with blue, purple: Vértesszőlős).

In case of the test measurements, the data acquisition was implemented by a high frequency LEMI-423 magnetotelluric station using 500 Hz sampling frequency. The sensors were installed under the surface ($\sim$0.5 m) and the data logger recorded the signals together with GPS timestamps. One vertical and two horizontal components of the magnetic field (B_X, B_Y, and B_Z) were measured by LEMI-120 induction coils. The telluric field components E_X and E_Y were observed between pairs of non-polarized Cu-CuSO4 electrodes placed 50 m apart. The field orientation of the magnetic and telluric sensors was set to the geomagnetic NS and EW directions. The signal from the induction coils is fed into a built-in amplifier. Local feedback circuits in the amplifier ensure that the transfer function of the system is fairly flat within the frequency band from 1 to $\sim$1000 Hz. The analog output from the electronics is sampled by a 24 bit A/D converter (LEMI-423 document, 2017).

The raw binary data files collected during the field measurements were transformed to text files, data were bandpass filtered (by applying the built in butterworth bandpass filter of the scipy.signal Python package) in the 4-40 Hz frequency range and dynamic spectra were generated with 1-min time and ~ 0.25 Hz frequency resolution for each day of the measuring campaigns. The visual inspection of the dynamic spectra allowed us to get a general impression about the ELF noise conditions at the test sites.

The 8 considered MT measurements were carried out from April to July in 2019 (Tab. I) and were recorded by a LEMI-419 data acquisition system with 640 Hz sampling frequency. For evaluating the detectability of SRs in the MT measurements, the same data processing steps were applied as for the field measurements. These records were usually less than 2 hours long.

Table I: Date, location and exact coordinates of the 8 MT measurements.

Date	Location	Coordinates
2019.04.08.	Mihályfa	17.19402° E, 46.96285° N
2019.04.10.	Réde	17.91118° E, 47.39947° N
2019.04.16.	Balatonújlak	17.34578° E, 46.65665° N
2019.04.25.	Porpác	16.77927° E, 47.24524° N
2019.05.08.	Magyarpolány	17.54579° E, 47.21791° N
2019.05.23.	Ráckeve	18.89396° E, 47.16264° N
2019.06.12.	Vértesszőlős	18.4016° E, 47.6357° N
2019.07.24.	Pécsely	17.8017° E, 46.9654° N

Results

The first, 24 hour long test measurement at Hortobágy indicated the suitability of the site for carrying out high quality ELF measurements while the second campaign unequivocally verified the low ELF noise conditions (Fig. 2) and confirmed the detectability of clear ELF spectra by our recording system. 5-6 SR bands can be recognized in these spectrograms up to 38 Hz. However, the test site at Hortobágy was more than 400 km away from Sopron (Fig. 1) which would make the regular maintenance and occasional repairing of a permanent station very difficult. Therefore, we attempted to find another location closer to Sopron with ELF noise
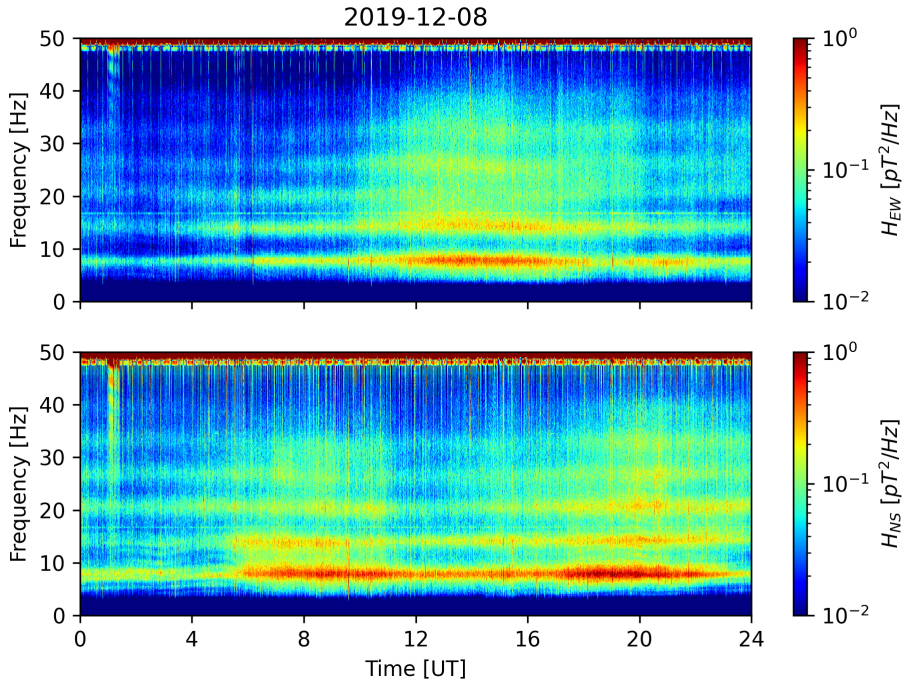
conditions ideally as good as at Hortobágy.

Fig. 2: Dynamic spectra corresponding to the H_{EW} (top panel) and H_{NS} (bottom panel) field components measured near Hortobágy on the 8th of December 2019.

In order to gain a more general knowledge about the ELF noise conditions in Hungary, we reprocessed the MT measurements described in the previous section. This analysis revealed that it is possible to collect high quality ELF data in more locations in Hungary but one needs to find a place at least 10-20 km away from electrified railway lines. As an example for the noise contamination, Fig. 3 shows power spectral density (PSD) spectra corresponding to ∼ 1 hour long records (in the same hour of the day: 13-14 UT) from the MT station near Vértesszőlős as well as from the field measurements near Hortobágy and Magyargencs. Despite the apparently different amplitude transfer characteristics of the LEMI 423 and 419 detection systems, it is clear that there is more explicit noise contamination at Vértesszőlős than at Hortobágy. This high noise level is probably caused by the nearby electrified railway line running less than 5 km away from the measurement site in that case. Based on this experience, we selected a location near Magyargencs, Hungary for our next test measurement.
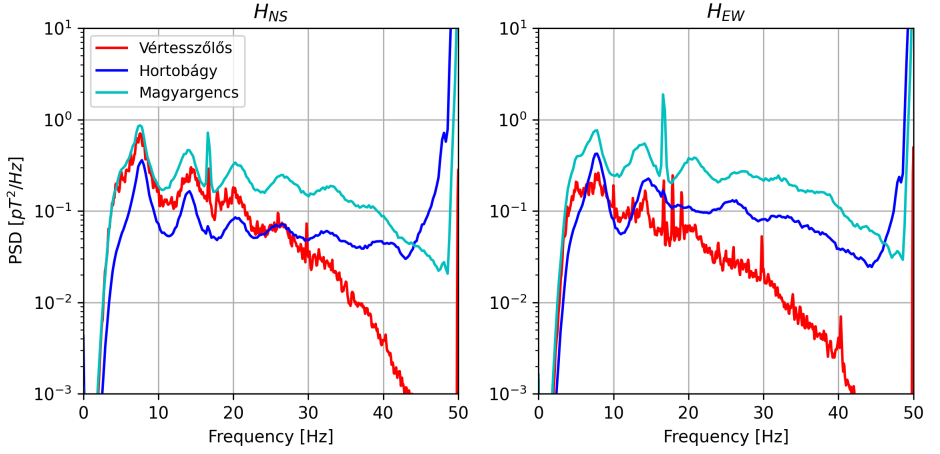
Fig. 3: PSD spectra corresponding to ~ 1 hour long records from Vértesszőlős, Hortobágy and Magyargencs.
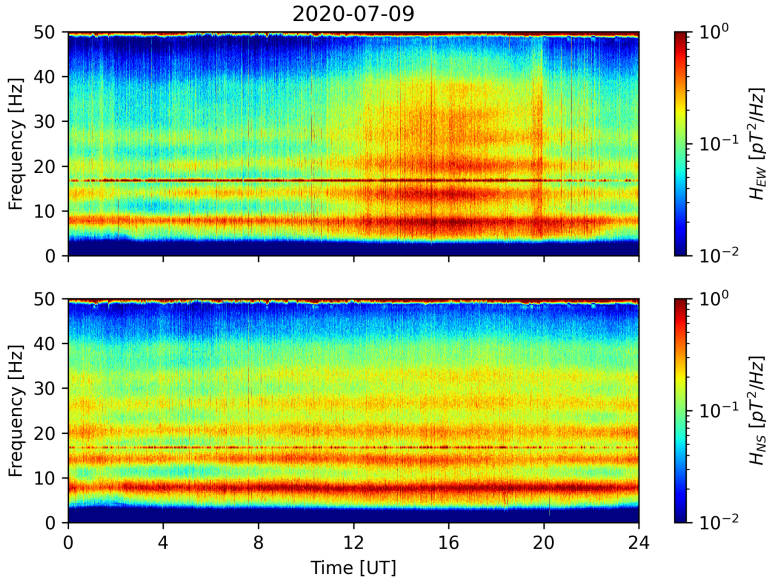

Fig. 4: Dynamic spectra corresponding to the H_{EW} (top panel) and H_{NS} (bottom panel) field components measured near Magyargencs on the 9th of July 2020.

Figure 4 shows very clear dynamic spectra corresponding to the H_{EW} and H_{NS} field components from the 9th of July 2020 measured at our second test site, near Magyargencs. The first five SR modes are clearly visible in the H_{NS} field component (bottom panel) while the dynamic spectrum of the H_{EW} field component (top panel) shows the expected characteristic daily pattern, namely a remarkable intensification between 13 and 18 UT corresponding to the intensification of the African lightning chimney (Williams et al., 2021). This figure confirms that the test site is appropriate for carrying out SR measurements. The higher signal levels compared to those recorded in wintertime at the first test site, Hortobágy, (Fig. 3), can be attributed to the fact that main centers of lightning activity are closer to the test site in summer. Note that, in addition to the seasonal variation, SR signal levels and peak amplitude ratios also change hour-by-hour and day-to-day according to the actual distribution and intensity of the global thunderstorm activity (Sátori et al., 2013).
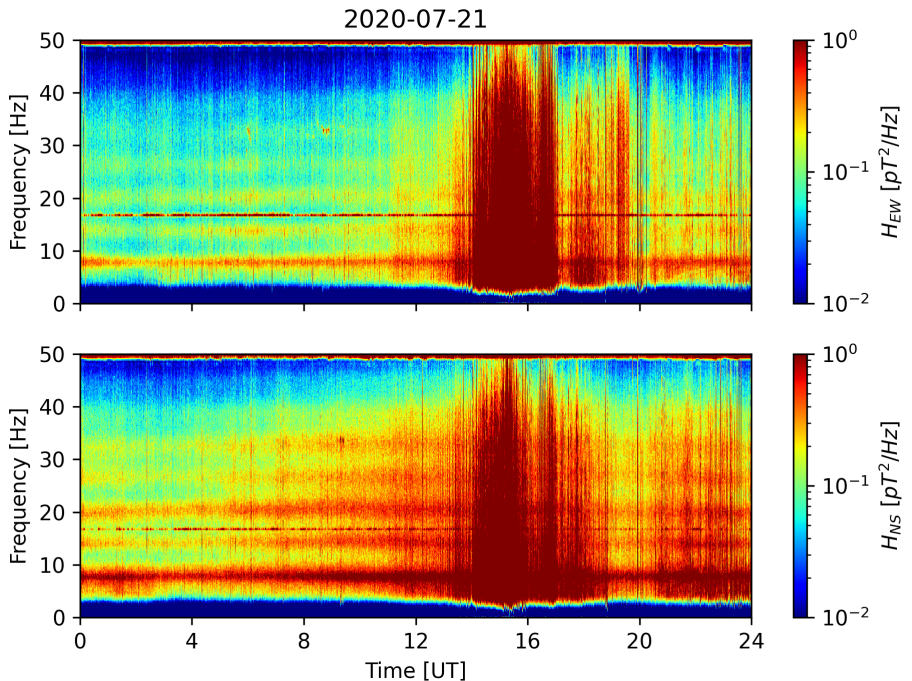

Fig. 5: Dynamic spectra corresponding to the H_{EW} (top panel) and H_{NS} (bottom panel) field components on the 21st of July 2020.

Such clear dynamic spectra are relatively rare in summer months when the fingerprint of local thunderstorms often appear as strong intensifications in the ELF spectra. This situation is demonstrated in Fig. 5 which shows dynamic spectra

from the 21st of July 2020. The effect of local lightning activity, appearing as very strong intensifications in the dynamic spectrum of both magnetic field components, is clearly visible between 14 and 17 UT. After 17 UT, strong intensifications appearing as individual (distinguishable) vertical lines are probably connected to regional lightning activity (Tatsis et al., 2021). Nevertheless, the dynamic spectra show clear signatures of the SR in the morning which again confirms desirable ELF noise conditions at the test site.

Note the particularly strong, constantly present signal at $50/3 \approx 16.67$ Hz in both field components (Figs. 3, 4, and 5). This signal is produced by the power system that serves electrified railway lines in Austria (Ogunsolar & Mariscotti, 2013). This signal is more or less present in ELF-band records taken at any location to the west from River Danube in Hungary but it may also appear in measurements done further to the east. Fortunately, the frequency of this artificial signal lies between two SR modes and can be handled by digital filtering techniques fairly well.

Summary

The location of the test measurement near Magyargencs seems to be an appropriate place to establish a site for making magnetic SR measurements. It is not known yet if the location is good for making SR measurements in the vertical electric field component, too. This is to be determined yet. As there is neither electric power supply nor internet access point in the area, any measurement must be run on batteries and the collecting of the recorded data requires regular personal visits to the site. These aspects also need to be considered before the establishment of the measurement site is decided.

Acknowledgements

References

Bór, J., Sátori, G., Barta, V., Szabóné-André, K., Szendrői, J., Wesztergom, V., Bozóki, T., Buzás, A., & Koronczay, D. (2020). Measurements of atmospheric electricity in the Széchenyi István Geophysical Observatory, Hungary. *History of Geo- and Space Sciences, 11*(1), 53-70, https://doi.org/10.5194/hgss-11-53-2020

LEMI-423, 2017. Wide band magnetotelluric station LEMI-423 technical description and operation manual. Laboratory for Electromagnetic Innovation, Limited Liability Company, LVIV

Ogunsola, A., & Mariscotti, A. (2013). *Electromagnetic compatibility in railways.* Dordrecht: Springer Science+Business Media. https://doi.org/10.1007/978-3-642-30281-7

Sátori, G., Rycroft, M., Bencze, P., Märcz, F., Bór, J., Barta, V., Nagy, T., & Kovács, K. (2013). An Overview of Thunderstorm-Related Research on the Atmospheric Electric Field, Schumann Resonances, Sprites, and the Ionosphere at Sopron, Hungary. *Surveys in Geophysics, 34*, 255-292, https://doi.org/10.1007/s10712-013-9222-6

Tatsis, G, Sakkas, A., Christofilakis, V., Baldoumas, G., Chronopoulos, S.K., Paschalidou, A.K., Kassomenos, P., Petrou, I., Kostarakis, P., Repapis, C., & Tritakis, V. (2021). Correlation of local lightning activity with extra low frequency detector for Schumann Resonance measurements. *Science of The Total Environment, 787*, 147671, https://doi.org/10.1016/j.scitotenv.2021.147671

Williams, E., Bozóki, T., Sátori, G., Price, C., Steinbach, P., Guha, A., et al. (2021). Evolution of Global Lightning in the Transition from Cold to Warm Phase Preceding Two Super El Niño Events. *Journal of Geophysical Research: Atmospheres, 126*(3), e2020JD033526, https://doi.org/10.1029/2020JD033526

Geomagnetic observation system in the Széchenyi István Geophysical Observatory

István Lemperger[1*], Judit Szendrői[1], Csongor Szabó[1], Lukács Kuslits[1], Árpád Kis[1], Sándor M. Szalai[1], Csaba Molnár[1] and Viktor Wesztergom[1]

[1]Institute of Earth Physics and Space Science (ELKH EPSS), Sopron, Hungary

Abstract

Geomagnetic and geoelectric registration has been continuously executed in SZIGO for more than six decades. The Observatory is a member of the global network of the geomagnetic observatories, the so-called INTERMAGNET (www.intermagnet.org). The geomagnetic observation system has recently been renewed in all of its components and the organically related geoelectric measurement system is going to be upgraded and improved, too. Present paper provides a short summary of the new geomagnetic observation system and introduces a few SSC events registered in the SZIGO from the last 12 months via the new observation station.

Keywords: geomagnetic observation, INTERMAGNET.

Introduction - motivation

In the early sixties two antimagnetic houses had been built for the geomagnetic measurements, one for the continuous recordings (called relative house) and the other for the measurement of the geomagnetic absolute values (called absolute house). They were built from limestone, the roof from reed. The continuous recording of the geomagnetic components H, D and Z, and the weekly measurement of the absolute value of these elements were started in July, 1960. The instrumentation was: two variometer sets of the type La Cour (made in Denmark) recording to 30×40 cm photo-paper sheets, two QHM-s (quartz-horizontal-magnetometer), one BMZ (balance-magnetic-zero) (also made in Denmark), a magnetic declinatorium and an Earth inductor (Askania). The magnetic declinatorium originally served in the Observatory Ógyalla, then in Budakeszi and in Tihany, but was later replaced by a magnetic theodolite in Tihany. Nevertheless, it was a very accurate instrument. The conventional magnetic instruments were used until 1989. From 1989

---

*Corresponding author: István Lemperger (lemperger.istvan@epss.hu)

till 1991 the measurements of magnetic absolute values were executed utilizing a vector proton magnetometer developed in the Observatory Niemegk. Since 1991 absolute measurements have been preformed by a triaxial fluxgate magnetometer and a proton magnetometer (ELSEC 820). Digital recording of the geomagnetic variation was also started by an ARGOS system (by the British Geological Survey) in 1991. The analogous photographic recording was run parallel during about one year.

Observatory reports of geomagnetic data has been published each year since 1961. As the observatory had in the first times the main aim of the continuous monitoring of the Earth's electromagnetic field of external origin, the chapter Geomagnetism was compiled in coincidence with the chapter Earth Currents. Telluric data is proved to be a very useful supplementation of the geomagnetic registration providing direct information about the local induction effect of the surface geomagnetic variation.

The activity indices reported were determined according to a linear scale, which increased by 7 nT broad steps. Only monthly and yearly averages of the absolute values of the elements were provided. The observatory has belonged to the INTERMAGNET cooperation since 1993. In the first years data were transmitted via METEOSAT satellite and later it has been improved to be transferred by regular email service to geomagnetic information nodes and made also available to the international research community on CD ROM and downloadable from the INTERMAGNET home page.

The co-ordinates of the observatory:

3-character IAGA code: NCK,
Geographic co-ordinates:
$\Phi = 47°38'$ (N),
$\lambda = 16°43'$ (E),
Altitude = 153.70 m (magnetic house),
McIllwain L = 1.9.

The low sampling rate of the geomagnetic variation (one data per minute) was proved to be insufficient to draw conclusion on the source ionospheric current systems and the ultimate magnetospheric phenomena. Thus demand for further improvement of the system has arisen.

Description and commissioning of the new measurement system

To develop and build an accurate and long run reliable, sufficient measurement system the components of the chain had to be selected in a prudent and thorough manner.

The first element of the chain is **the host building** itself which has originally been built utilizing only non-magnetic parts. The so-called relative house's roof has

been renovated 2 years ago. The core of the system is a 3-axis **fluxgate magnetometer model FGE** by DTU Space which has a proven track-record at many observatories worldwide. It is easy to set up and operate and has demonstrated baseline stability over decades. The FGE has analog outputs enabling the user to adapt the instrument to their own data logging systems. Main features of the system are as follows:

- 3 linear core fluxgate sensors mounted on a marble cube for good mechanical stability.

- Bias and feedback coils on quartz tube for high temperature stability.

- Highly stable digitally controlled compensation of main field. Very good long-term stability.

- Magnetically very clean electronics which may be placed rather close to the sensor head.

- Temperature sensors in the FGE-sensor head and the electronics.

The next step in the process is the analogue/digital conversion. This task is performed by a **SYMRES USB8CH** 24 bit real-time continuous data acquisition system with an individual A/D per channel architecture. Suitable for sampling from DC to 10 kHz, an on board 4 MB FIFO guards against any data loss even on heavily interrupted and multitasking computers. Sitting outside the PC for improved noise performance, the system communicates its acquired data to the computer via a standard USB port. All analog inputs are fully differential with amplitude ranges of $\pm$ 4 V. The data is processed and stored on a **BeagleBone Black** microcomputer by the platform independent software environment provided by SYMRES. Full featured acquisition programs like DVM and Scope are included with the system software easily controlling acquisition rates and continuously saving acquired data to disk. The pipelined architecture allows simple customization of the provided programs. For developing custom utilities, low level pipeline functions are supplied.

The microcomputers are equipped with industrial quality 16 GB SD cards to secure the reliable data acquisition for long turn. The original flexible pipeline has been supplemented by some extra scripts for automatic quasi real-time data service to an INTERMAGNET GIN and direct real-time data forwarding to a separated high performance **computer/data server** by local network. The last element of the data acquisition system is the server which stores the second sampled geomagnetic data in an SQL database with separated tables for each day and one table for the last 24 hours data. Archived data includes the GPS time stamp, 3 geomagnetic components (X, Y, Z), the sensor temperature (Ts) and the temperature of the electronics (Te) leaving open the possibility of a subsequent temperature correction.

The power of the whole system is supplied from a 12 V 74 Ah battery continuously fed by the central solar power system of the Observatory. Clone system is archived on backup memory card for case of emergency to secure the permanent data acquisition.

Registered events

(Storm) Sudden Commencements (SSC) are defined by an abrupt increase or decrease in the northward component of the geomagnetic field, which marks the beginning of a geomagnetic storm or an increase in activity lasting at least one hour. The sudden commencements and solar flare effects (SFE) are from magnetograms of the worldwide network of magnetic observatories.

The stations, together with their abbreviations, are given in the series IAGA Bulletin No. 32 which contains the yearly compilation of these data. Before January 1966 these reports were published periodically in Journal of Geophysical Research. From then until 1970 they were published quarterly in Solar-Geophysical Data (SGD). Beginning with December 1970, these data are published monthly and, thus, are based on fewer reports and differ slightly from similar data published previously. The decision to publish this less complete report was made in order to make the data available more rapidly. Only events reported by at least five observatories are reported.

The latest SSC reports are provided by Observatorio del Ebro, Roquetes, Spain, on behalf of the IAGA Service on Rapid Magnetic Variations, see Curto et al. (2007).

Seven reported events which can be definitely identified in the SZIGO data from the last 12 months are listed in Table I. and as they appear on the SZIGO registration are demonstrated on Fig. 1-7.

Table I: Reported SSC events based on data of at least five geomagnetic Observatories in the last 12 months.

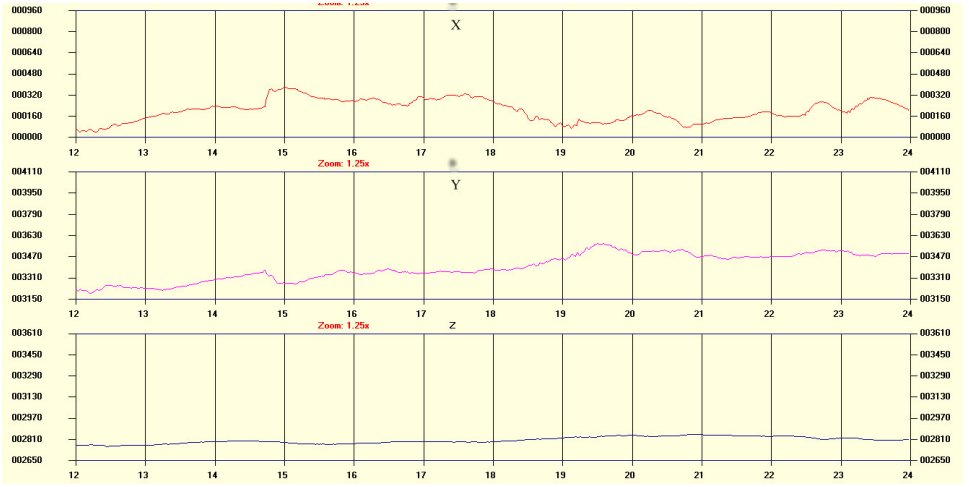| YYYY	MM	dd	hh	min	Amplitude (nT)					Qualification					Type
2020	10	19	14	41	13.4	9.5	14.7	21.1	22.1	3	2	2	2	3	SSC
2020	10	23	13	20	7.3	7.3	11.4	11	10.8	0	1	1	1	1	SSC
2020	12	10	2	9	20.2	18.5	19.5	25.1	21.8	3	3	3	3	3	SSC
2021	5	12	6	37	27.7	25.5	20.7	46.3	36.4	2	3	2	3	3	SSC
2021	5	26	12	44	13.1	25.1	17.9	20.8	26.9	3	3	3	3	3	SSC
2021	6	2	13	30	8.8	9.8	11.6	13.3	14.8	1	1	2	3	2	SSC
2021	8	27	1	14	12.4	12.8	17.5	12.1	15.7	2	1	1	1	2	SSC

Fig. 1: SSC event identified on SZIGO geomagnetic registration – 19-10-2020 (H, +13.9 nT).
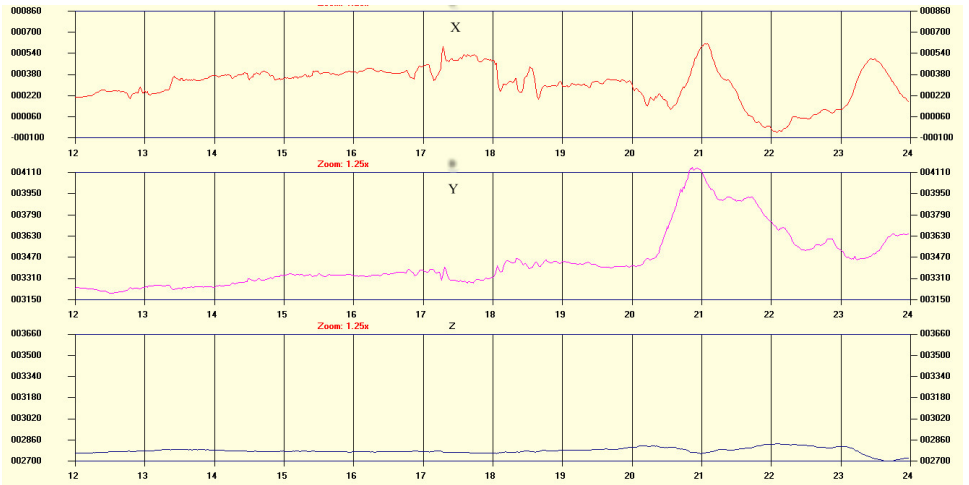

Fig. 2: SSC event identified on SZIGO geomagnetic registration – 23-10-2020 (H, +10.2 nT).
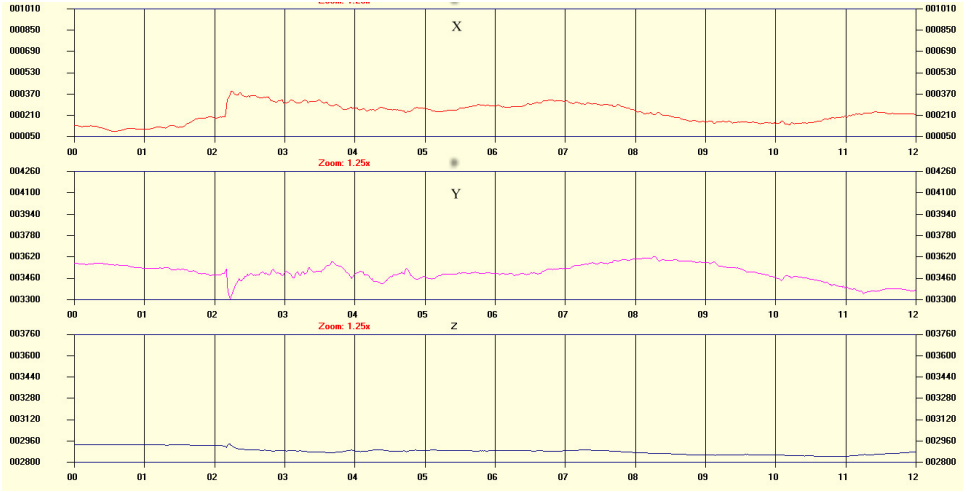
Fig. 3: SSC event identified on SZIGO geomagnetic registration – 10-12-2020 (D, −22.4 nT).
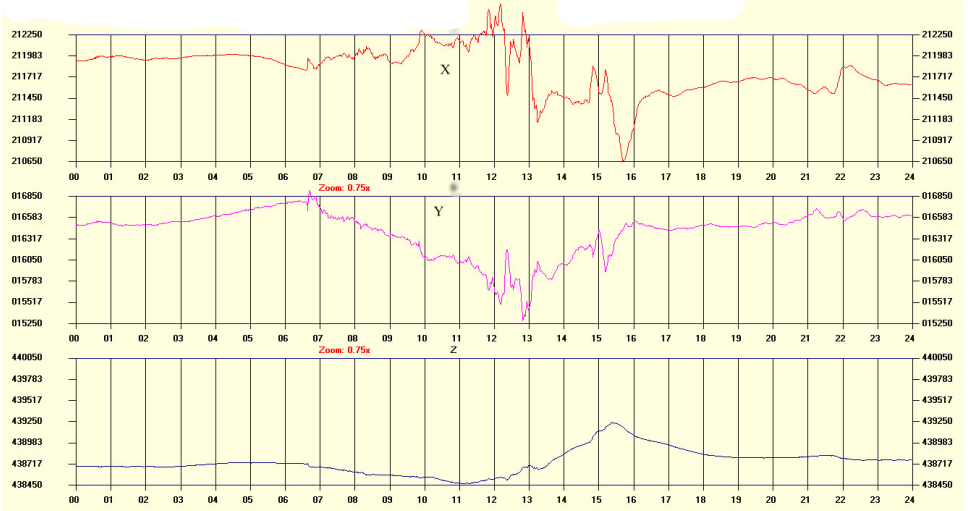

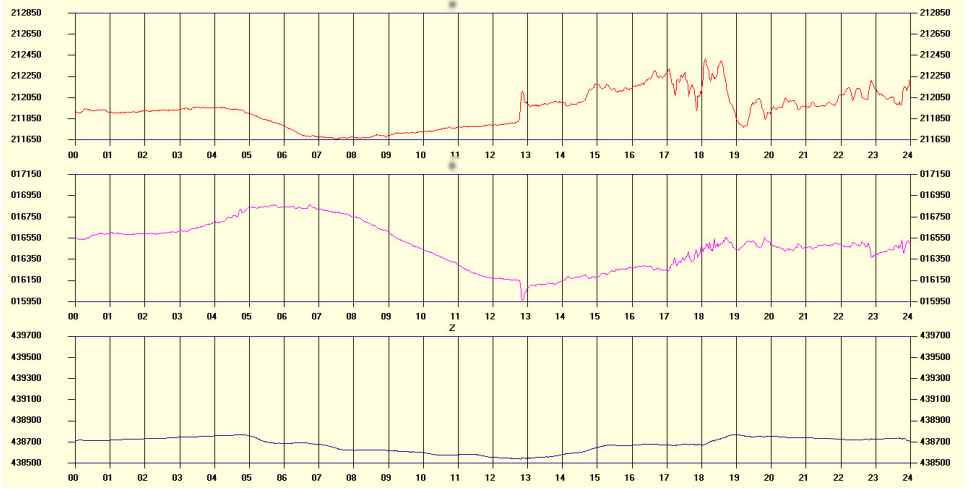**Fig. 4:** SSC event identified on SZIGO geomagnetic registration – 12-05-2021 (D, +26.0 nT).

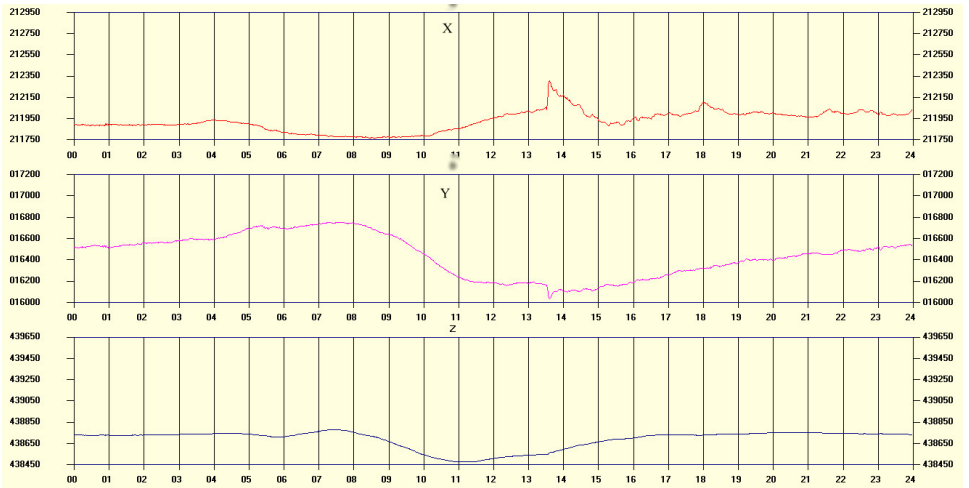**Fig. 5:** SSC event identified on SZIGO geomagnetic registration – 26-05-2021 (H, +29.1 nT).

Fig. 6: SSC event identified on SZIGO geomagnetic registration – 02-06-2021 (H, +27.6 nT).
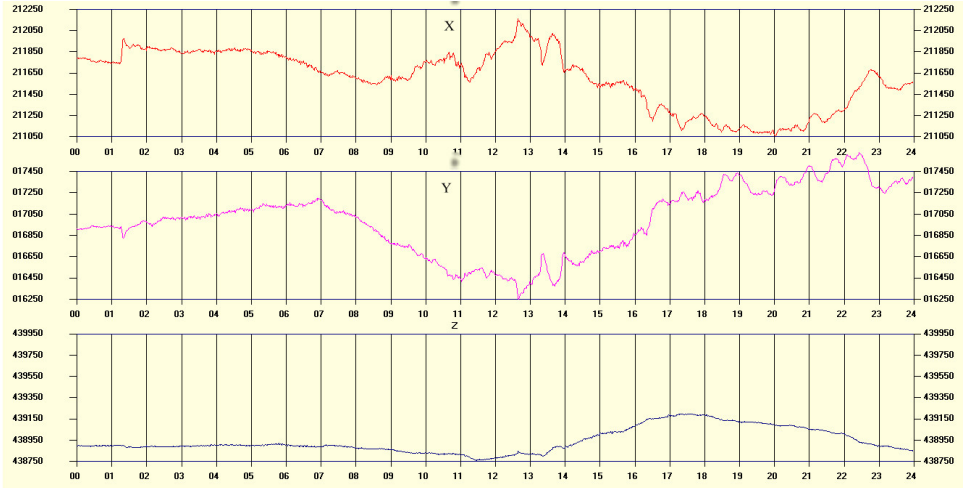
Fig. 7: SSC event identified on SZIGO geomagnetic registration – 27-08-2021 (H, +24.2 nT).

Future prospects

A unique laboratory facility is under construction in the Observatory area in cooperation between Wigner Research Centre for Physics and Institute of Earth Physics and Space Science (Erdős et al., 2019a,b). The main goal of the investment is the implementation of a laboratory environment with an efficient compensation and effective additional shielding of the surface geomagnetic field, eliminating not only the static part, but the external origin dynamic component, too. The quasi real-time second sampled geomagnetic data access is essential for the accurate control of the active compensation system. Furthermore, the geomagnetic and telluric observations will also be accessible within the Space Weather Data Center under construction.

The reconstruction of the permanent geoelectric data acquisition system is also in progress with the intention of increasing the sampling rate, dynamic range and securing data storage, remote access of the telluric registration.

References

Curto, J. J., Araki, T., & Alberca, L. F. (2007). Evolution of the concept of Sudden Storm Commencements and their operative identification. *Earth, Planets and Space, 59*, pp. i–xii, https://doi.org/10.1186/BF03352059

Erdős, G., Hevesi, L., Lemperger, I., Nagy, J., Nemeth, Z., & Wesztergom, V. (2019, May 20-22). *Installation of an Electromagnetic Test Facility in Hungary* [Paper presentation]. 2019 ESA Workshop on Aerospace EMC, Budapest, Hungary. https://doi.org/10.23919/AeroEMC.2019.8788935

Erdős, G., Hevesi, L., Kuslits, L., Lemperger, I., Lichtenberger, J., Németh, Z., U. Nagy, L., Veres, M., & Wesztergom, V. (2019, April 24-26). Mágneses Nulltér Laboratórium (ZBL) létrehozása. [Paper presentation] In: *Magyar Űrkutatási Fórum 2019 - Az előadások összefoglalói.* Magyar Űrkutatási Fórum 2019, Sopron, Magyarország. http://urforum.ggki.hu/docs/MUF2019_abstract_book_final.pdf#page=29

Automatic display of ELF measurements recorded in the Széchenyi István Geophysical Observatory

Karolina Szabóné André[1*], Tamás Bozóki[1,2], József Bór[1], Csongor Szabó[1] and Gabriella Sátori[1]

[1]Institute of Earth Physics and Space Science (ELKH EPSS), Sopron, Hungary

[2]Doctoral School of Environmental Sciences, University of Szeged, Hungary

Abstract

From July 2020, ELF data recorded in the Széchenyi István Geophysical Observatory (SZIGO, IAGA code: NCK) near Nagycenk, Hungary is automatically displayed on the website of the observatory (http://nckobs.hu/data/sr/). The automatically generated figures contain the dynamic spectra of the H_{NS}, H_{EW} and E_Z field components as well as the amplitude and frequency of the first three Schumann resonance (SR) modes as extracted by the complex demodulation algorithm from the E_Z record. This important achievement allows us to continuously monitor the actual state of the measurements. Currently, the figure corresponding to the actual day is accessible for the public while the archive of figures is available only for the staff of the research institute. The number of people visiting the website is continuously tracked and the statistics confirm that there is considerable public interest in our measurements.

Keywords: Schumann resonance, extremely low frequency, data processing, data visualization.

Motivation

At the SZIGO, continuous monitoring of AC phenomena in the global electric circuit, specifically the Schumann resonances (SRs), started in the early 1990s with the installation of a ball antenna (Sátori et al., 2013; Bór et al., 2020). The system was upgraded with induction coil magnetometers in 1996. The complex demodulation algorithm was selected as an adequate algorithm to extract the modal frequency and the amplitude of the first three SR modes (Sátori et al., 1996). Only these spectral parameters were stored until 2003 when the system was upgraded to save the digitized raw time series as well.

---

*Corresponding author: Karolina Szabóné André (szabone.a.karolina@epss.hu)

Probably due to the senescence of the recording system, there were more and more problems with the measurements in the recent few years, which raised the need for the continuous monitoring of their actual state. Furthermore, quick-looks are usually standard, freely accessible data products at many geophysical observatories (like at the Sodankylä Geophysical Observatory, https://www.sgo.fi/) so we decided to develop our own process for displaying ELF records automatically on the website of the observatory.

Implementation

The automatic plotting program processes raw data files of .fw4 file extension every 10 minutes. These files are obtained using a Symmetric Research (SymRes) 4-channel data logger. The program is started by a scheduled task running a batch file. The batch file executes a Python code, which performs the complex demodulation and calculates spectra from 10-minute long data series. The end of the processed time period is always 5 minutes earlier than the start of the actual program run. The spectral parameters for the dynamic spectra are calculated from each .fw4 file using 10 s long time windows slid by 5 s between calculations. Then, the 1-minute averages are calculated and saved into three .csv files (one for each data channel). The amplitudes and frequencies of the first three Schumann resonance modes, calculated only for the E_Z field component via the complex demodulation algorithm, are saved to another .csv file. The program creates the .csv files at the beginning of each day and appends data to them every 10 minutes. Then, the data from the .csv files are read and plotted.

The north-south (NS) component of the magnetic field is measured by the induction coil which is the original instrument that was installed on-site in 1996. Since November, 2016, the east-west (EW) component is measured by a LEMI-120 type magnetic antenna that has been installed because the corresponding other original induction coil had to be replaced. Note that the two magnetic antennas have different sensitivities and transmission characteristics. To have a good view on the operation of the signals from both antennas, the color scale for each plot was set up differently. The maximum value of the color scale of the spectrogram of the signal from the EW-oriented (old) coil is 57% higher than that from the NS-oriented LEMI coil.

The automatically generated plot has five subplots (Fig. 1). The first three subplots show the dynamic spectra of the H_{NS}, H_{EW} and the E_Z field components, respectively. The last two subplots show the results of the complex demodulation: the amplitudes and the frequencies based on the E_Z component. The frequencies of the first three SR modes are about 7.9, 14.1 and 20 Hz, respectively. To plot them on one subplot, three y axes were set up as it is indicated by different colors.

The plot is saved to a .png file whose name is always the same. This .png file is uploaded to the nckobs.hu web page via ftp connection and it is displayed on the web page. At the end of the day, the .png file which shows data from all day is saved with a filename which contains the date of the actual day. Then, this file is also uploaded to the nckobs.hu for internal use. Additionally, it is also uploaded to
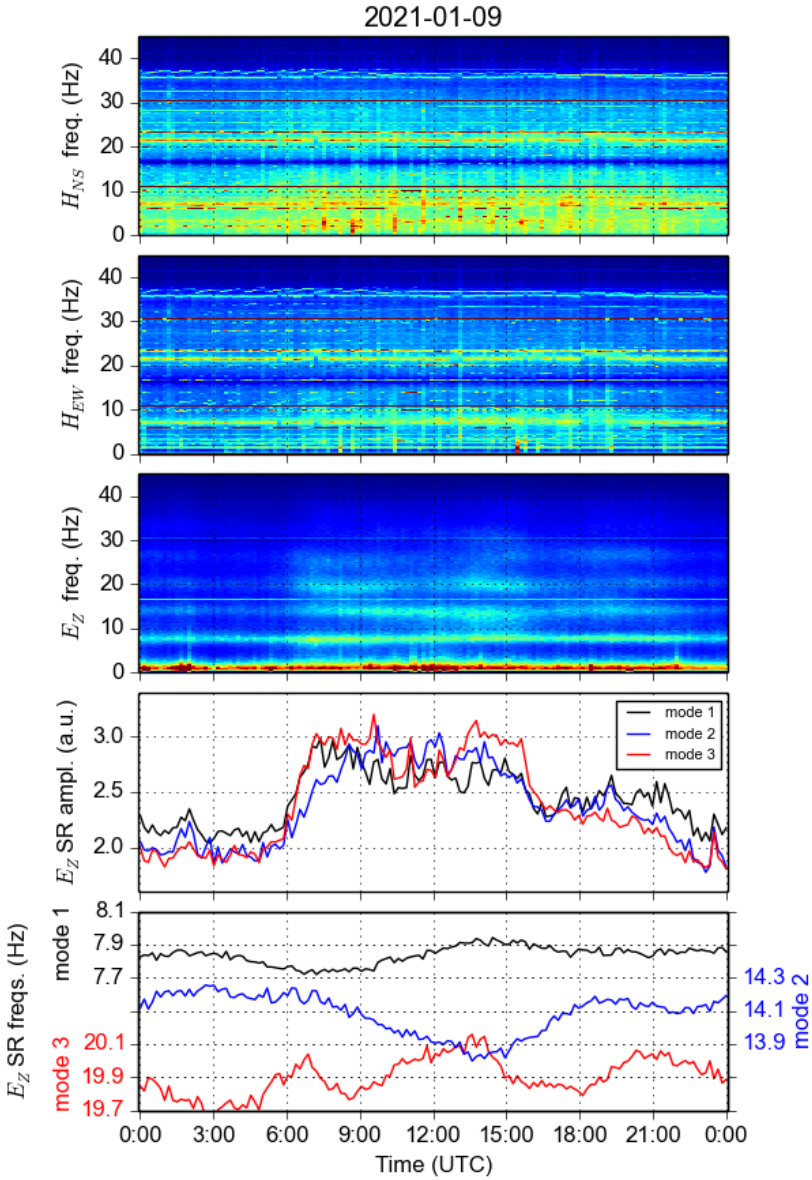
Fig. 1: The automatically generated figure showing the Schumann resonance measurements at the SZIGO on the 9th of January, 2021.

a NAS storage, next to the archived data files.

The program is set to send a warning email when the amplitudes and frequencies can not be calculated via the complex demodulation because the signal from the ball antenna is lost. The program also sends an email when the signal is received again.

The information mirrored by the picture

The primary role of the produced plot is that it helps to check that the SR measurement is working correctly. The color scales are set so that the plot shows SR peaks well when the local environment for the measurements is quiet, i.e., there is no strong wind, precipitation, or nearby thunderstorms in which strong electrical activity takes place in the ELF band, too. If the local environment is disturbed, mechanical vibrations of the antenna or strong ELF-band signals cause that the SR pattern is not visible due to the noise of high amplitude. In these cases, the complex demodulation method cannot work properly and either it produces biased values or cannot provide any output at all. Therefore, the curves and values on the plot produced by the automatic data processing code should not be considered as a reference. The data and results need verification and quality check before any interpretation is made or conclusions could be drawn.

Spectrograms on the upper three panels (Fig. 1) demonstrate well that SR in the vertical electric field component in the SZIGO can be measured very well. Apart from the usual natural and few artificial disturbances, the SR pattern is well detectable. One characteristic of the noise of human origin is that it usually starts and ends suddenly. This allows the primary separation of artificial and natural noises as the latter tend to develop and ring down more gradually. One annoying noise of artificial origin in the E_Z signal is produced by the electric power management in the observatory due to the applied solar panels. This artificial signal appears for a few tens of minutes near dawn and dusk when the operation of the batteries is switched (Fig. 2).

Figure 1 and 2 also show that the horizontal magnetic field in the SZIGO is strongly contaminated by both narrow band and wide band noises so that SR cannot be detected most of the time in the corresponding signals. Occasionally, the noise level is lowered for short time periods of a few hours so that the first or second SR modes can be recognized in the H_{EW} field component (Fig. 2). This shows that noise levels in the ELF band in the SZIGO are direction dependent. Most probably horizontal electric currents cause the strong noise in the magnetic field in the SZIGO. These electric currents can flow horizontally in the upper layers of the ground and their source is most probably the imperfect, leaky grounding of the power system that serves the traffic on the electrified railway lines running in a distance of only a few km to the south from the observatory.
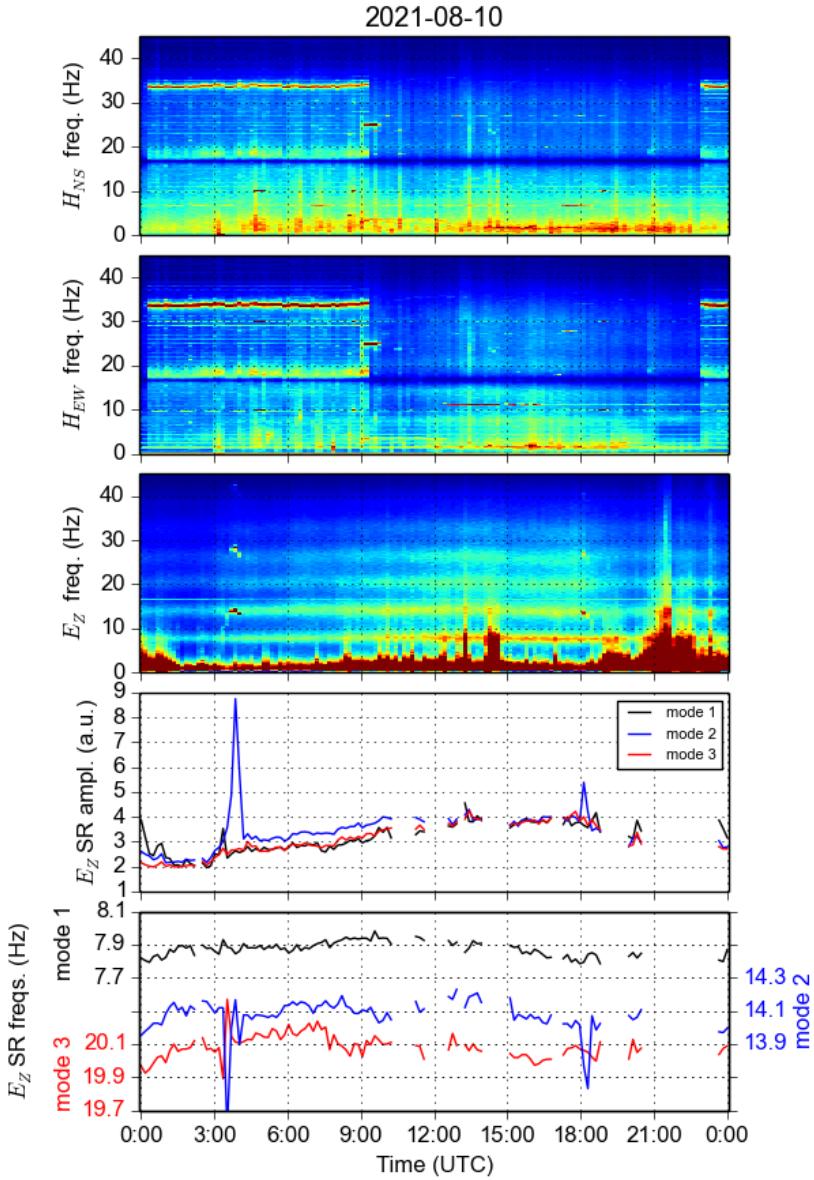
Fig. 2: The automatically generated figure showing the Schumann resonance measurements at the SZIGO on the 10th of August, 2021.

Visitor statistics

This paragraph presents some interesting information about the visitors of our web page (http://nckobs.hu/data/sr/) as seen on the 9th of September 2021. The visitor statistics are tracked using the free services of clicky.com. In the 28-day-long period from August 13, 2021 to September 9, 2021 our website has been visited 1149 times (excluding visits from our institute). Besides the number of visitors, the tracking program also collects information about their location. Most of the visitors in this 28-day-long period were located in Hungary (1054, 92%). Our website has been visited also from abroad, from the following countries (the number of visitors are shown in the parenthesis after the name of each country): Slovakia (17), Austria (16), Romania (14), United Kingdom (12), Germany (9), USA (6), Croatia (5), Serbia (5), Czech Republic (4), France (2), Belgium (1), Ireland (1), Spain (1), Switzerland (1) and The Netherlands (1). The large number of visitors confirms that there is considerable public interest in our measurements.

Acknowledgements

References

Bór, J., Sátori, G., Barta, V., Szabóné-André, K., Szendrői, J., Wesztergom, V., Bozóki, T., Buzás, A., & Koronczay, D. (2020). Measurements of atmospheric electricity in the Széchenyi István Geophysical Observatory, Hungary. *History of Geo- and Space Sciences, 11*(1), 53-70, https://doi.org/10.5194/hgss-11-53-2020

Sátori, G., Rycroft, M., Bencze, P., Märcz, F., Bór, J., Barta, V., Nagy, T., & Kovács, K. (2013). An Overview of Thunderstorm-Related Research on the Atmospheric Electric Field, Schumann Resonances, Sprites, and the Ionosphere at Sopron, Hungary. *Surveys in Geophysics, 34*, 255-292, https://doi.org/10.1007/s10712-013-9222-6

Sátori, G., Szendrői, J., & Verő, J. (1996). Monitoring Schumann resonances – I. Methodology. *Journal of Atmospheric and Terrestrial Physics, 58*(13), 1475-1481, https://doi.org/10.1016/0021-9169(95)00145-X

Conception of a computer monitoring and function-specific remote controlling application framework

József Bór[1*] and Csongor Szabó[1]

[1]Institute of Earth Physics and Space Science (ELKH EPSS), Sopron, Hungary

Abstract

An idea is described for the implementation of a framework by which the operation of a computer can be monitored and controlled remotely. Main advantages of the proposed solution are that (1) it can be implemented using open source code and applications, (2) remote monitoring and control can be made using a general web browser, (3) the operation does not need large bandwidth internet connection, (4) it gives system administrators complete control over the production, format, and appearance of the content that serves monitoring purposes, (5) remotely controllable operations can be fully customized, and (6) the proposed remote controlling solution does not make the supervised computer more vulnerable for hacker attacks. The proposed application framework can be an optimal solution for monitoring and remote controlling computers that manage data acquisition from different measurements or run programs which require occasional user intervention.

Keywords: remote control, computer management, operation monitoring, content sharing, automatization.

Introduction

The possibility of monitoring and controlling a computer remotely has many practical advantages, e.g., checking proper operation of the system and programs, supervising the activity of users, providing help, sharing information, or simply working without the need of being physically near the hardware. Users usually want as complete access as possible to the functionalities and settings over which they possess rights in a specific system. For system administrators, this means complete control over the computer while for normal users, this means the same regarding the range of services available within their accounts.

---

*Corresponding author: József Bór (bor.jozsef@epss.hu)

The most straightforward concept of remote monitoring/accessing a computer is direct access to the system over the internet. In this model, a service (that provides access) is running on the computer and clients connect directly to the system through this service. Several applications and communication protocols have been developed in this sense to allow remote access to a computer (Comparison of remote desktop software, 2021). Advanced applications can be set to allow partial access to the system to limit the risk of malicious usage. This means either allowing solely view-only access or providing possibilities to use/monitor only specified applications. This is called application sharing (Taylor, 2020).

Applying this solution has several pitfalls. Opening direct access to a computer always raises the risk of becoming the victim of hacker attacks. The service itself must be configured carefully. Service programs use optimized data transfer methods and often proprietary communication protocols so that the user does not know how these programs work and has limited control on what information is transmitted. Setting up direct access may require additional configuration if the computer is located behind a firewall, e.g., port forwarding (How to Port Forward, 2021). This is not always easy (or can be even impossible) to realize when the user has no rights to configure the firewall (e.g., in a company or university). Note that the issue regarding firewalls can be solved by tunneling the transferred information through an independent web service (Tunneling, 2021). The maintenance of such servers, however, is costly so that such solutions are usually provided as a paid service. This solution may not be suitable for users having trust concerns because the operation depends on a third party server and all transmitted information is channeled through such a server. Several service applications have their corresponding specific client software the installation of which may also cause inconveniences under different operating systems (Comparison of remote desktop software, 2021).

Another approach concerns mostly content-sharing needs, therefore it can be considered as a monitoring solution. This model, too, requires a service installed on the system. In this case, the task of the service is to upload or stream the content to be shared to a server and users/viewers can reach the information by connecting to the server rather than to the content-providing (CP) computer. This solution is safe because it does not rely on incoming requests to the CP system. Firewall issues are rare because the upload is initiated from inside by the information-providing system. Nevertheless, difficulties in setting up such solutions may come up because installing and configuring a server correctly as well as creating the corresponding user interface requires specific knowledge. Well established content-streaming applications and corresponding web-based services are available for live-sharing popular content such as audio and video (List of streaming media systems, 2021). These solutions are optimized to these content (media) types and may generate considerable data traffic. They often require wide band internet connection. The nature of this approach does not allow direct control of the CP system.

Here we conceptualize the framework which allows either monitoring and/or controlling a computer remotely, is relatively easy to set up, eliminates firewall issues, and is not content-specific. The motivation of considering the development of such a solution is triggered by the need for being able to monitor the operation of

different measurements running in the Széchenyi István Geophysical Observatory (IAGA code: NCK) (Bór et al., 2020) and, occasionally, changing some settings as required. Another specific field of possible application is enabling co-workers and citizen scientists to remotely supervise and manage a computer-controlled optical observation system built for observing upper atmospheric electro-optical phenomena. The monitoring part consists of obtaining and organizing text and images of different formats from different sources/programs in the CP system regarding the various measurements. On the other hand, controlling of the recording systems may consists of starting and stopping different applications, changing settings and making various complex actions (minimizing/maximizing windows, mouse clicking buttons, capturing the screen, etc.). This should be achieved without allowing a user to have complete control over the full functionality of an application or the system. One or few applications that handle all these tasks could be coded and users could be allowed to fully control only these applications using application sharing solutions. We propose a more universal and transparent solution to this problem so that the content to be remotely seen and the actions that can be initiated remotely can be completely and easily customized.

Fundamentals of the proposed framework

In the proposed framework for remote monitoring and management of computers, the content-providing (CP) system is separated from the content-sharing (CS) system. The CP system is a computer, possibly behind a firewall, while the CS system is supposed to be a public web server. Remote users connect to the web server with a general web browser and see the uploaded actual information or may interact with the web server if the content is interactive. The information on the web server is kept up to date by the CP system, from where the latest information is uploaded to the server regularly. In the implementation of controlling functionality, the CP system also queries the web server for user requests.

Content management on the supervised computer

One key part of the proposed solution is a content manager (CM) routine that is scheduled to run periodically on the CP system. The routine completes a few main tasks. The order of completion of the tasks can be arbitrary, nevertheless, keeping the following order is recommended. One main task can be querying the web server for requests from the remote user. If there are requests, the routine starts the execution of the corresponding actions. The routine also starts the execution of code and commands which provide output to be shown for the remote user (monitoring functionality). The routine then refreshes the content on the CS system.

The CM routine can be launched regularly using the task scheduler service that is usually available on the operating system, or can be embedded in a program loop within the CM application. The first solution is preferred if the goal is only monitoring and the information of interest is refreshed rarely. Using the system's

task scheduler imposes too much load on the system if the content needs to be refreshed frequently. If the usage is of such, setting up the CM routine in a program loop is preferred. It is also easier to start and stop a single application than to configure system-level settings or services. Note that a single application, too, can be configured to run as a service so that continuous operation of the application can be guaranteed if needed.

In a practical implementation, the CM routine runs the CP code and applications by cycling over batch files in a single directory. The order of the names of the batch files can determine the order of execution. This way, the actions can be overviewed easily, the order of execution can be changed simply by renaming the batch files appropriately, and tasks can be created or removed simply by adding or deleting batch files, respectively. This also has the advantage that the CM framework does not need to be edited directly.

Care must be taken not to start programs that run for a long time or can freeze and block the running of the CM routine. It is suggested that long running or unstable programs be started as a separate process in the background. It can be a good practice to insert a code in the beginning of the corresponding batch file that checks if the previously started program is still running. If the process is still running, it can be either killed before it is run again or starting it can be skipped either completely or at least for a given time-out interval.

It makes it easier for the CM routine to manage the content produced by the applied code and programs if the output of those applications is directed to a single directory. It is suggested that the content is to be produced in 'web-ready' format so that the CS system on the web server does not need to process it further and so the remote user can view the information as it gets uploaded. Another advantage of this implementation is that the content can be checked also locally. Note that local installation of a web server may be necessary for a local user to be able to verify the functionality of the content if it has interactive parts. Including active code in the web content is highly suggested so that the information in the remote user's browser can be automatically refreshed (ajax methods) (Zhaoyun et al., 2010; Faang, 2021) without the need for manual re-loading the page. Note that browsers or corporate firewalls may store previously downloaded web content in a cache (Caching Behavior of Web Browsers, 2014). This may cause that, for example, an image does not change in the remote user's browser although it has already been refreshed on the web server. If the name of the updated image remains the same, the browser may not recognize the change and keeps reloading the latest image from the cache instead of the new file on the server. This behavior can be avoided by passing a changing parameter (e.g. current time) along with the file within the HTML code (Lutkevich, 2020) so that the browser recognizes the change and always downloads the new file from the web server.

Especially if the monitored content is composed of several parts, changes quickly, and the refresh rate is high, producing the monitored content comes with many disk I/O operations. Initiating many disk I/O requests can not only cause slow program operation, but it also speeds up wear out of the hard disk (Wu et al., 2018). In case of such requirements, and if the size of the content as well as the available computer

memory (RAM) makes it feasible, it is suggested to use a virtual RAM disk (RAM Disk, 2021) for collecting the newest version of the monitored content.

On the other hand, the internet traffic corresponding to uploading the files to the CS web server can be lowered by keeping track of the files in the monitored content and by uploading only those that are new or have changed. This can be implemented by creating verification codes of the uploaded files on the web server using a hashing algorithm (CRC, MD5, etc.) (Basatwar, 2021). By comparing those codes to the corresponding codes of the actual files on the CP system, synchronization of the content on the web server can be limited to the changed information: uploading new files, deleting those that are not present anymore, and replacing those that have changed.

Handling remote requests on the supervised computer

If remote control is needed, it is a task of the CM routine to query the CS system on the web server for new requests from the remote user and to manage the completion of those requests. This functionality can be part of the duty cycle for the monitoring part but it can also be implemented independently. The advantage of the latter is that querying the web server is not restricted to the refreshing interval set for the monitoring CM routine. Instead of that, the 'long polling' technique (Faang, 2021) can be used which maintains a communication channel between the managed computer and web server. The same technique can be applied regarding the communication between the remote user and the web server. This results in quick refreshing of the information in the remote user's browser whenever the content on the web server is changed. Regarding the controlling functionality, requests from the remote user can be instantly received and processed as well as simple responses can be sent back to the remote user via the CS system if this technique is applied.

To keep track of the status of the remote requests, it is suggested that they are to be downloaded to a specific folder on the controlled system (e.g., a folder named 'requests_received') with an attached identifier (e.g., timestamp) so that the time order of their execution can be unambiguously determined. The requests themselves are supposed to be text messages consisting of a command word and optional arguments. For each requestable valid command, a batch file can be created (supposedly with an identical name) so that the CM routine can easily parse the requests and will handle only those that have a corresponding executable batch file. The CM routine should cycle over the downloaded requests. If a request is valid, the CM code runs the corresponding batch file with the requested arguments and copies the request entry to another folder named, e.g., 'requests_processed' along with its direct return value (text). Note that the concerns about long-running and hanging processes should be considered when the request-processing batch files are coded. Also note that it is completely valid for request-processing programs to also create output in the folder where the content produced by the system-monitoring scripts is collected. That way, the corresponding results can appear in the monitoring section of the application, too.

Finally, the CM routine should upload the content of the folder 're-quests_processed' to the web server so that the remote user can follow the course of actions. If the upload completes successfully, the requests can be archived for book-keeping purposes in another folder named, e.g., 'requests_archived'. That way, the received requests, their order of execution and their direct simple return messages can be reviewed simply and easily any time locally on the supervised computer.

Creating and registering new commands the execution of which can be requested can be implemented in a fairly user-friendly way. The CM routine can be coded to check the list of request-processing batch files regularly. This way, the validity of the received requests can be checked against the actually available list of functionalities. This strategy ensures that only valid requests are accepted from the remote user in a way that service files on the CS system need not to be modified at all.

The suggested solution ensures that remote operation is fairly safe as only those commands can be run remotely for which the implementing batch file exists on the controlled system.

It may be worth considering adding a security feature to the code on the web server to ensure that routines there accept content only from the CP system. A simple solution for that is to pass a security code invisibly as part of all POST messages (Williams, 2021a) to the CS system on the web server. The validity of that code can be checked and any communication will be started only if the code is okay. Communication can be further secured by using secure HTTP protocol (HTTPS) (Friyanto, 2019; Williams, 2021b). When HTTPS is used, the information is transferred in an encrypted form so that it cannot be reconstructed even if it is captured.

Functionality of the code on the content-sharing system

The code on the CS system (web server) has three main roles. It receives the content to be shown from the CP system, it manages the communication with the remote user (i.e, it receives controlling requests), and it passes the received requests to the CP system upon being queried. If the content of the monitoring functionality is produced in a web-ready format, the code on the CS system does not need to process it further. The only task related to those files is the creation of their verification code via the selected hashing algorithm.

There are several details which are worth considering in the implementation of these functionalities. For instance, it can be advantageous from the point of view of compatibility in the communication if the code on both the CP and the CS systems is implemented using the same software framework (e.g., Python, PHP, Java Script, etc.). Regarding the handling of the requests of the remote user, it is suggested to set up a folder structure similar to that on the CP system. Remote requests are suggested to be saved in a folder named, e.g., 'requests_received', together with a timestamp. After these requests are transferred to the CP system, they can be moved to another folder named, e.g., 'requests_sent' so that, depending on the im-plementation of the user interface, it is possible for the remote user to follow their status. Once the requests are processed on the CP system, prompt results (ide-

ally bundled with the original requests) are suggested to be uploaded into another folder named, e.g., 'request_processed' and then the corresponding entries in the 'requests_sent' folder can be removed. The user interface should be able to show to the remote user both the actual status of the requests and the prompt simple messages they returned.

If the monitoring/controlling functionality is to be used by a single user, simple password protection of the access to the shared content and to the controlling interface may provide a sufficient level of security. Opening the usage of especially the controlling interface for multiple users requires additional considerations. To avoid confusion, it is suggested to allow only for one user at a time to control the CP system. The related functionality must be managed by the code on the CS system. A conception of a possible solution for handling multi-user access is given below.

Each user is supposed to have a unique username and a corresponding password. Once one of the users allowed to control the CP system signs in, its IP address would be registered. For that user, a controlling session starts so that the login interface is not further provided for other users who visit the login page from IP addresses different from that of the signed-in user. The time point of gaining control or the time point of the latest request sent (whichever is later) is recorded for the active user. If that user is inactive for a specified amount of time, the IP lock gets released so that other allowed users may log in and take the control over. It is advised that there be a supervisor who can always sign in and can take the control over. In case of multi-user implementations, it is suggested for bookkeeping purposes that the username be recorded together with each request sent.

Conception of a flexible content presenting framework

The proposed framework for a monitoring and remote controlling solution allows the administrator of the supervised computer to set up both the shared content itself and the appearance of the content on the web server completely freely. Nevertheless, designing and implementing a user-friendly web page which can handle automatic refreshing of the displayed content, not to mention the user interface for controlling requires specific knowledge. We propose a basic framework for the displayed content itself which can be easily used by an average computer user to set up any basic set of status-monitoring information.

The main idea behind the conception is that each bit of information to be shared has its own simple HTML code snippet which determines the appearance of the corresponding content (text, images, etc.). One or more of such code snippets together with its corresponding files (e.g., image files), if needed, can be generated by each batch file (or the process started by it) run by the CM routine on the CP system. The final web page containing all information is supposed to be compiled by a master code which incorporates all actually existing code snippets. The order of appearance of the content in the web page can be the alphabetical order of the filenames containing the HTML code snippets. This way, the user can determine the appearance of each part of shared information freely and independently from other content entries.

Summary

We described the conception of a general framework for remote monitoring and controlling the operation of a computer. The proposed solution gives the administrator of the supervised computer full control over both the content to be presented for monitoring purposes and its appearance. The framework is based on the idea that the remote user is connected to a web server where the presented content for monitoring and, optionally, the user interface for remote control is available (Fig. 1). The content on the web server is updated regularly by a content-manager routine running on the supervised computer. It causes no problem if the CP system is working behind firewalls since all communication between the web server and the supervised computer are initiated from the supervised computer and can be implemented using common HTTP or HTTPS protocols.
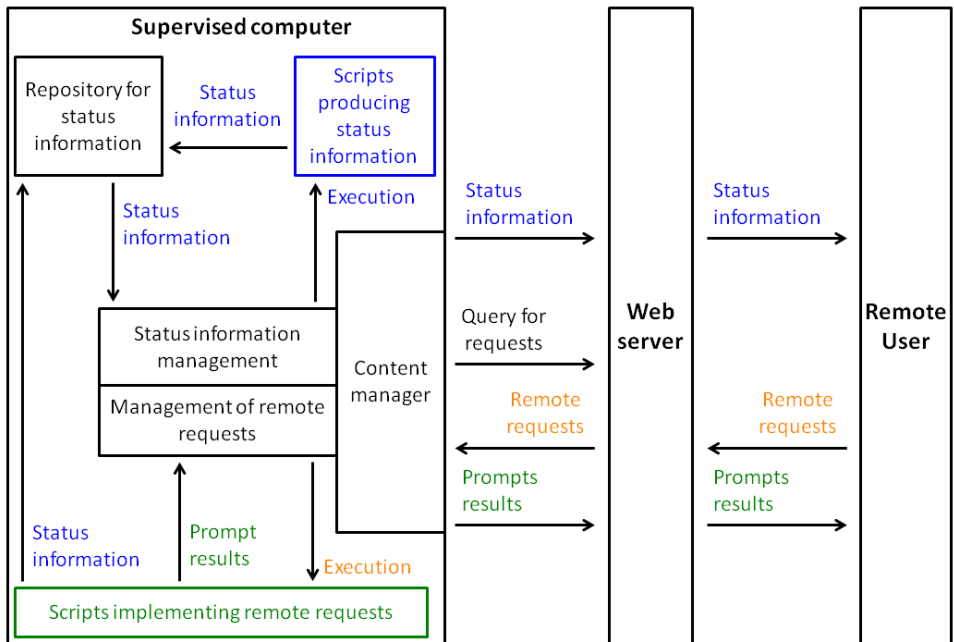

Fig. 1: Flow chart of the proposed monitoring and controlling application framework.

The framework may include the functionality of making specific operations on the supervised computer remotely controllable without opening any general purpose access channel to the supervised system. The proposed solution makes it possible that the set of remotely controllable options, functions, and services in the supervised computer can be fully and easily customized, reviewed, and managed by the administrator of the system. The framework itself, therefore, can be considered

very safe from the point of view of hacker attacks from the internet. Note that it is the responsibility of the administrator of the supervised system to allow only safe operations to be remotely requestable.

Finally, a general framework was suggested for easy management of various types and appearances of contents to be shown to the remote user via the web server. The main idea behind that framework is that files containing HTML code snippets are produced by each monitoring content-provider code or program and a master routine compiles these code snippets into a complete web page that appears in the browser of the remote user. Note that no parts of the proposed application framework require seamless internet connection. Should any communication attempt fail, it will be re-tried in the next refresh cycle.

Beside describing the general ideas, several aspects of the possible implementation are discussed including security-related questions and options for extending the framework to be used by more remote users. Realization of the proposed conceptions may uncover additional problems that need to be solved for the system to work optimally. Nevertheless, we are confident that a communication system that works basically according to the given guidelines performs well for the intended purposes.

Acknowledgements

References

Basatwar, G. (2021). Hashing Algorithms – An In-Depth Guide To Understanding Hash Functions. Retrieved November 30, 2021, from https://www.appsealing.com/hashing-algorithms/

Bór, J., Sátori, G., Barta, V., Szabóné-André, K., Szendrői, J., Wesztergom, V., Bozóki, T., Buzás, A., & Koronczay, D. (2020). Measurements of atmospheric electricity in the Széchenyi István Geophysical Observatory, Hungary. *History of Geo- and Space Sciences, 11*(1), 53-70, https://doi.org/10.5194/hgss-11-53-2020

Caching Behavior of Web Browsers (2014). Retrieved November 30, 2021, from https://www.f5.com/services/resources/white-papers/caching-behavior-of-web-browsers

Comparison of remote desktop software (2021). Retrieved November 30, 2021, from https://en.wikipedia.org/wiki/Comparison_of_remote_desktop_software

Faang, C. (2021). Ajax polling vs long-polling vs WebSockets vs server-sent events. Retrieved November 30, 2021, from https://medium.com/geekculture/ajax-polling-vs-long-polling-vs-websockets-vs-server-sent-events-e0d65033c9ba

Friyanto, A. (2019). Hyper Text Transfer Protocol for Securing Packet Inspection in Intrusion Prevention System Device. *IOP Conference Series: Materials Science and Engineering, 662*, 022021, https://doi.org/10.1088/1757-899X/662/2/022021

How to Port Forward – General Guide to Multiple Router Brands (2021). Retrieved November 30, 2021, from https://www.noip.com/support/knowledgebase/general-port-forwarding-guide/

List of streaming media systems (2021). Retrieved November 30, 2021, from https://www.wikiwand.com/en/List_of_streaming_media_systems

Lutkevich, B. (2020). HTML (Hypertext Markup Language). Retrieved November 30, 2021, from https://www.theserverside.com/definition/HTML-Hypertext-Markup-Language

RAM Disk (2021). Retrieved November 30, 2021, from https://www.techopedia.com/definition/2801/ram-disk

Taylor, N. (2020). The Collaboration Series: Chapter 4 – What Is Application Sharing? Retrieved November 30, 2021, from https://www.gamma.co.uk/resources/blog/what-is-application-sharing/

Tunneling (2021). Retrieved November 30, 2021, from https://www.speedcheck.org/wiki/tunneling/

Williams, L. (2021a). GET vs POST: Key Difference between HTTP Methods. Retrieved November 30, 2021, from https://www.guru99.com/difference-get-post-http.html

Williams, L. (2021b). HTTP vs HTTPS: What is Difference Between HTTP and HTTPS? Full Form. Retrieved November 30, 2021, from https://www.guru99.com/difference-http-vs-https.html

Wu, S., Yi, Y., Xiao, J., Jin, H., & Ye, M. (2018). A Large-Scale Study of I/O Workload's Impact on Disk Failure. *IEEE Access, 6*, pp. 47385-47396, https://doi.org/10.1109/ACCESS.2018.2866522

Zhaoyun, S., Xiaobo, Z., & Li, Z. (2010). The Web asynchronous communication mechanism research based on Ajax. *2nd International Conference on Education Technology and Computer*, pp. V3-370-V3-372, https://doi.org/10.1109/ICETC.2010.5529524

Remotely controlled observations of electro-optical upper atmospheric phenomena from Baja, Hungary

József Bór[1*], Tibor Hegedüs[2], Zoltán Jäger[2], Tibor Molnár[1], Csaba Molnár[1], Csongor Szabó[1], Karolina Szabóné André[1], Zoltán Zelkó[2] and László Döbrentei[3]

[1]Institute of Earth Physics and Space Science (ELKH EPSS), Sopron, Hungary

[2]Baja Observatory of the University of Szeged, Baja, Hungary

[3]Research Centre for Astronomy and Earth Sciences (ELKH CSFK), Budapest, Hungary

Abstract

A remotely manageable optical observation system for recording transient luminous events (TLEs) in the upper atmosphere was installed in Baja, Hungary in 2014. This report describes hardware components and settings of the system, software solutions applied either for realtime event detection and remote control, and the strategy of actually making the observations. An overview on the number and type of TLEs observed up to 2020 is presented. During the 7 years of operation, 1655 TLEs were recorded, 92.7% of which were red sprites, 6.4% were sprite halos, and the set of captured events contained altogether only 3 ELVES. Most sprites were observed in June while most sprite halos were observed in September over the years covered in this report.

Introduction

The existence of sub-ionospheric optical emissions of various peculiar forms and characteristic dynamics with durations less than a second were proved mostly in the late 80's and 90's. These phenomena are optically observable signatures of electrical excitation processes which take place in the atmosphere above the clouds of electrically active thunderstorms. As the parent processes that trigger the appearances of these phenomena are directly linked to fast charge transport in the thundercloud (i.e., intense charge separation and lightning strokes), we refer to these events as electro-optical upper atmospheric phenomena or transient luminous events (TLEs).

---

*Corresponding author: József Bór (bor.jozsef@epss.hu)

Present knowledge on physical processes behind the initiation and development of the various emission types, i.e., ELVES, red sprites, sprite halos, blue starters, blue jets, gigantic jets and upward lightning discharges is summarized in comprehensive review papers (Pasko et al., 2012; Siingh et al., 2012; Surkov & Hayakawa, 2020).

TLEs provide an alternative way to study extreme lightning activity in thunderstorms and chemical as well as physical interactions including electrodynamic coupling processes in the upper atmosphere (Siingh et al., 2011; Gordillo-Vázquez & Péter-Invernón, 2021). This explains why efforts are made worldwide to register the occurrences of these events using both ground-based recording facilities and space-borne observations (Hsu et al., 2017; Neubert et al., 2019; Arnone et al., 2020).

Organized observations of TLEs from Hungary started in 2007 in Sopron to serve scientific research (Bór et al., 2009; Bór, 2013; Bór et al., 2018). The site provides fairly good observational coverage in middle Europe over Hungary, Slovakia, the Czech Republic, Austria, south-east Germany, south Poland, Slovenia, Croatia, the northern part of Serbia and Bosnia, and the western part of Romania (Bór et al., 2009). Especially during autumn and winter, however, lightning activity is more pronounced over the Mediterranean region (Arnone et al., 2020). To cover more area to the south of Hungary in these time periods, a second observation system was set up in the south part of the county in Baja in 2014 (Fig. 1). In this report, we briefly describe the hardware and software components of the system as well as the methodology which is applied in the observations. Then, observations made since the installation of the system up to the year 2020 are summarized.

The site: Astronomical Observatory in Baja

The observatory (46.180278° N, 19.010833° E, 110 m above mean sea level) is about 4 km away from the city center of Baja, close to the southern border of Hungary. The corresponding area is about 4 ha large. It is a protected area and the light pollution is low. The building of the observatory was constructed in 1981 and the astronomical research staff moved here from the city centre in 1986. From this time on, the original scope of research in Baja that addresses studying the upper atmosphere on the base of satellite observations (Ill, 1983) has been extended to include classic stellar astronomy. The only telescope in the observatory between 1985 and 1992 was a 40 cm Cassegrainian reflector (property of the University of Szeged) and photometric observations of selected eclipsing binaries were made almost each clear night (Hegedűs et al., 1992). Following a period of uncertainties in financing, a new main telescope (50 cm f/8.4 RC) was installed in Baja in 1995. The development of a large-field telescope (50 cm refractor, f/6) started in 2005. This instrument has become the first Hungarian robotic photometric telescope with an SDSS filter system. Based on this telescope, a new observation program, the BASSUS supernovae program (Vinkó et al., 2012) has been initiated by the University of Szeged. This has led to setting up a new 80 cm f/7 RC robotic telescope in 2020 in the observatory. Presently, the main activity in the observatory is related to supernovae research as well as observations of eclipsing binaries and multiple star
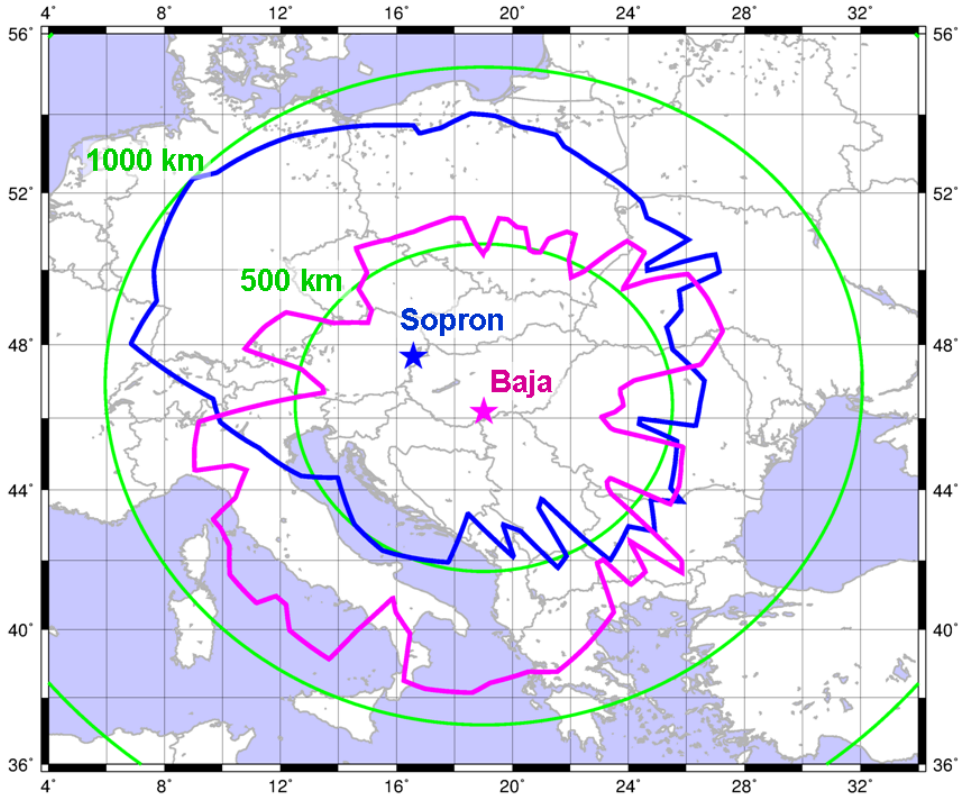
Fig. 1: Observational coverage for watching above 50 km altitude from Baja and from Sopron.

systems (Mitnyan et al., 2018). Beyond these main directions of astrophysical research, the area of scientific activities in Baja includes more multidisciplinary fields of studies like meteor science or near-Earth space phenomena. TLE observations fit well into these new lines. Figure 2 shows the building of the observatory with the camera mounted on the roof.

Components of the optical observation system

Hardware components of the optical part of the observation system in Baja are similar to those that have been used in Sopron (Bór et al., 2009), but there are minor differences. The camera is of the same type as that in Sopron, i.e., a Watec 902H2 Ultimate (1/2", CCIR). On the camera, uniform backlight area is set (the default state), electronic shutter is switched off and the auto exposure (AE) mode is set to position 8 where the exposure index (EI) is off and the lowest shutter speed is 1/50 s. Gamma is set to LO ($\gamma \approx 0.45$). Manual gain control mode is selected

Fig. 2: Baja Astronomical Observatory with the TLE camera on the roof (zoomed-in image is on the inset).

and the gain is set to have the noise level and the brightness of the acquired picture balanced. This way, relatively faint events can be detected without having too many false detections due to large noise fluctuations.

The camera is equipped with a Tamron 12VG412ASIR aspherical, IR corrected lens in Baja. The maximum f-stop value of this lens is 1.2. The focal length of the lens was set so that the effective size of the field of view (48° horizontally, 35° vertically) is similar to that in Sopron. Experience shows that this setup provides a fairly wide viewing angle and, at the same time, fairly detailed images of TLEs. Analog video signals are channeled through a video time inserter (TIM-10) to have a time stamp on each video frame so that the start and end of the exposure time of each video half frame (covering 20 ms) can be read directly with millisecond accuracy. The signals are digitized in the recording computer by a Leadtek WinFast VC100XP PCI digitizer card in a standard resolution of 720x576 pixels.

During observation, consecutive digitized video frames are evaluated realtime by the UFO Capture event detection software (version 2.22). The software is set to trigger on the simultaneous brightening of 15 pixels or more. To detect brightening reliably and still be able to capture faint events, noise tracking is enabled in the software and the ratio of the detection level to the noise level is set only to 105% with a minimum difference of 2 units required between them. It was found that the gain on the camera is close to optimal when the detect level is at around 40-45 units during normal monitoring without any event occurring. The corresponding gain

setting was found by experience. To reduce the number of false detections due to cosmic ray events that brighten up only a few pixels in just one frame, the minimum duration for an event to raise a normal trigger (parameter 'Min(frm)') was set to 2 frames. At the same time, the minimum number of brightened pixels that maintain this state (detect size) was set to 2 to record even very small events of relatively longer duration. Additionally, irrelevant parts of the actual view (e.g., buildings, trees, and the overlaid time stamp) as well as failing pixels of the camera CCD were masked out. The dark object mask feature was enabled at level 2, identification of slow objects (e.g. airplanes) was turned on (highest speed 15, size 15), and the scintillation mask option was switched on (level 105, speed 2, size 5). This latter setting allows the software to detect and register stars, which are the most common scintillating objects in the night sky. A utility software was developed to distinguish static scintillating pixels (usually due to CCD degradation) from stars, the position of which changes on the image with time. Note that the position of the camera should not change in the evaluation period. Other scintillating pixels are masked and the stars can then be used to determine the actual direction of the camera and the events within the field of view very accurately. Once a trigger had been raised, a short clip of the event was recorded with 10 frames both before and after the triggering video frame.

Remote controlling of the observations

The optical system can cover only a limited part of the sky at a time. Areal coverage can be extended by using a pan-tilt solution to aim the camera above actually active thunderstorms occurring in any direction and distance within the observable distance range. A unique, weather resistant, remotely controllable camera-directing solution was developed and installed in Baja for the first time. The system is based on a Videotec PTH-355P pan-tilt unit (PTU) with which the camera can be moved by DC motors and the actual pan and tilt positions can be determined from analog signal outputs. A controlling electronics was developed to serve as an interface between the PTU and the computer that runs the detection software. It provides the user with the possibility of changing the position of the camera as needed. The system can set the azimuth and elevation angle of the camera with an accuracy of $0.1°$. The electronics allows the user to switch on or off heating in the camera house to lower the relative humidity in the camera house. Additionally, controlling the electronic iris on the lens can be taken over from the camera and the iris can be set to stay fully open or closed. While automatic iris control can save the CCD from being exposed to very strong light directly for a long time, this feature of the controlling electronics is very useful in cases when the reaction time of the automatic iris control is slow or when disturbing lights in an irrelevant part of the picture would otherwise cause the iris to close so that fainter events would be missed. Note that only a $338°$ wide azimuth range can be set on the PTU. In spite of that, the full $360°$ azimuth range is covered because the wide field of views of the camera overlap at the two end-azimuth positions. All functions of the PTU-controlling electronics can be accessed through serial connection using a simple RS232 terminal program.

The data acquisition PC, the camera, and other hardware parts of the system don't need to be switched on all the time. To allow switching on and off these devices as needed, a power switch was developed which can be controlled remotely and independently from other units in the detection system through a web interface. The power switch is based on a SR-201 2-way Ethernet relay board, the capability of which has been extended so that it can manage the powered state of 8 different devices.

A PC is used to control all units in the detection system. This control includes setting up and running the event detection software, directing the camera, heating of the camera house, and setting the state of the iris. Note that the power switch can be controlled independently from the PC. Video clips and observation logs are collected locally and some of the pre-processing tasks are also carried out on that computer. These complex tasks require the observer to have full control over the PC. Application of the Tiger VNC software was found to be a bandwidth-friendly solution that is proved to serve this need reliably. To save the camera from strong daylight, an algorithm was created and implemented in PHP coding language to shut down both software and hardware components of the observations system properly and automatically. The code is scheduled to run around surface sunrise times at Baja.

Methodology of the observations

TLEs can be detected during the night in low-light conditions when scattered sunlight doesn't mask the relatively small number of photons emitted during these events. TLEs appear above thunderstorms in which charge separation processes are very active (Pasko et al., 2012). Therefore, it must be determined whether there are active nighttime thunderstorms anywhere within the area above which the height range of typical TLE occurrences (e.g., 50-90 km for red sprites) can be fully observed from the recording site. This range is determined from images on which the horizon around the site is visible. After the direction of the camera is determined by matching the stars in the image to the sky map at the time point when the image was taken, the elevation of points right above the horizon is determined at several azimuths. Finding these elevations can be accomplished by using the UFO Analyzer program. Then, the maximum distance within which one can see the atmosphere only above any given altitude can be calculated (Fig. 3). Note that the curvature of the Earth must be taken into account. These distances depending on the azimuth border the covered area around the site (Fig. 1).

Occurrence of active thunderstorms can be forecasted. A forecast can be found on the webpage of the European Storm Forecast Experiment project (ESTOFEX, 2021). Actual presence of active thunderstorms within the covered area can be checked on realtime lightning maps which are produced by a number of services and can be found at several websites (left panel on Fig. 4). Some examples are BlitzOrtung (2021); LightningMaps (2021); Meteologix (2021).

Satellite images showing infrared (IR) cloud top temperatures are another useful source of information (AllMetSat, 2021). On one hand, the development and time
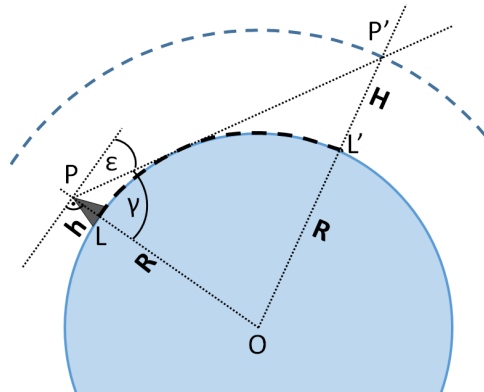
Fig. 3: Geometry for determining the range LL' from the point of observation P at a height h above main sea level within which one can see the atmosphere above the altitude H above main sea level. The radius of the earth is R and ϵ is the elevation angle of the horizon in P. First, γ must be calculated and then the POP'Δ needs to be solved for the LOL' angle using the law of cosines.

evolution of the active thunderstorm cells can be followed by monitoring the series of IR images. Active cells feature intense updraft in which moist air is lifted towards the upper troposphere where it cools down and clouds form. This process can be seen in the images as rapidly appearing and extending, rather localized white spots of very cold cloud tops (Schmetz et al., 1997) (right panel on Fig. 4). On the other hand, IR images can give a hint whether there are any clouds between the observation site and the region of interest. Such clouds may block the view and can make successful observations impossible. Note that the clouds move and transform fairly quickly and the cloud cover is not necessarily continuous, so it in fact happened that TLEs were recorded between clouds or through discontinuities of the cloud cover. In any case, local viewing conditions must be good. In Baja, this can also be checked using all-sky images from an independent camera which is installed locally. The number of stars visible closely above the horizon indicates well the presence of long-distance visibility. The more stars can be seen, the better the viewing conditions are.

Red sprites are a type of TLEs which are most often recorded by common optical systems in ground-based observations (Arnone et al., 2020). Therefore, the camera is usually set to capture these events with high probability. The appearance of sprites is triggered by intense positive cloud-to-ground (+CG) lightning strokes (van der Velde et al., 2014). Sprite events are known to appear at various distances behind the convective cores above the stratiform region of the thundercloud in the mature state of the thunderstorm (Soula et al., 2015; Bór et al., 2018; Wang et al., 2019). While the location of thundercloud cells of deep convection can be estimated

and the extension of the stratiform cloud region can be guessed from satellite IR images, the most reliable sources of this information are weather radar composite images. One service where radar images can be found is the radar animation service from Eumetnet (Saltikoff et al., 2019)[†].
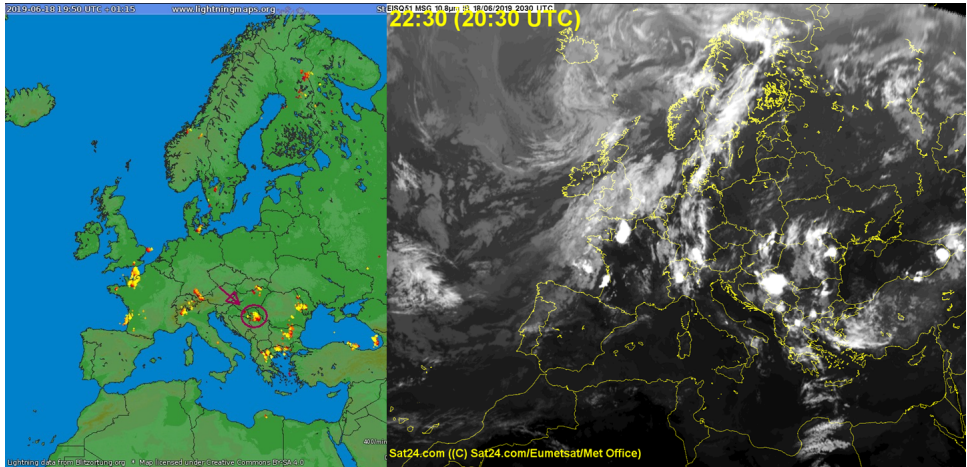

Fig. 4: Resources for determining the location of active thunderstorms. **Left:** Lightning map from BlitzOrtung/Lightningmaps.org. The storm cell which produced TLEs that were recorded in Baja is marked. **Right:** a corresponding Meteosat IR cloud top temperature image.

In practice, the observer first checks if there are any potentially TLE-producer thunderstorms within the observable area. If there is at least one storm of such and the local viewing conditions are good, the camera is turned on and will be directed toward the most promising storm so that both the active cells and the corresponding stratiform region of the storm to be within the horizontal viewing angle. The elevation angle of the camera must be chosen so that as thick height region below the altitude of 100 km to be covered as possible (Fig. 5).

If an observer is available to make observations on a night, the following information is logged: presence or absence of potentially TLE-active thunderstorms within the covered area, any circumstance that may interfere with successful observations (e.g., intervening clouds, poor local visibility, system malfunction, etc.). If any observations are made, the camera positions and system commands (e.g. switching on and off the camera, or iris control) are logged by the directing system. In addition to the video clip of each recorded event, the UFO Capture software saves the actual scintillation map and brightness peak-hold image of the video clip along with an

---

[†]https://www.eumetnet.eu/activities/observations-programme/current-activities/opera-radar-animation/
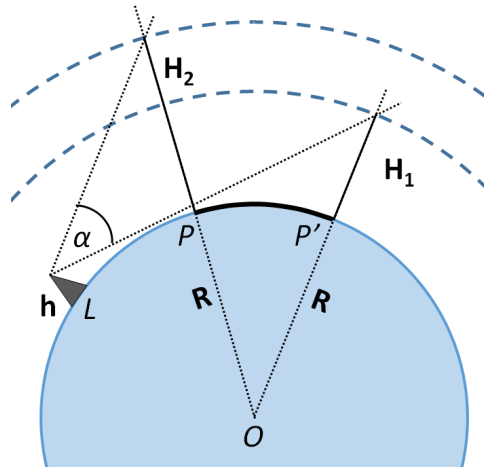
Fig. 5: A limited distance range PP' from the observer in location L is covered fully by a camera of a given vertical viewing angle α if an altitude range between heights H2 and H1 is to be monitored.

XML file containing the parameters with which the program was operated.

During initial post-processing, the events are reviewed one by one to identify TLEs. Then, the appearance time of the event is extracted from the time stamps in the video clip and the type of the TLE (red sprite, sprite halo, ELVES, etc.) is identified by visual inspection. Finally, the area of TLE production is determined roughly for distinct periods of TLE production which are clearly separated from one another by longer pauses (about 30-40 minutes) in the occurrences of events. Bordering coordinates of the production area are read in a resolution of 0.5° or 1° (depending on the ambiguity of the case) from lightning maps on which cumulated lightning activity in the TLE production period is displayed.

Overview of the observations from 2014 to 2020

During the first 7 years of operation, altogether 1655 different TLEs were recorded by the camera in Baja. The vast majority of the events were red sprites (1535), but sprite halos also were detected (106). Only 3 ELVES were recorded and the set includes 4 more events the type of which could not be identified unambiguously. The left panel in Fig. 6 shows the number of recorded events in each year. Note that these events were recorded on different numbers of nights in those years, so the average number of observed events on a night gives a somewhat better impression on the general intensity of sprite production in a year. This is shown on the right panel in Fig. 6. Note that the standard deviations are almost always greater than the mean value which indicates that the corresponding distribution is not normal.
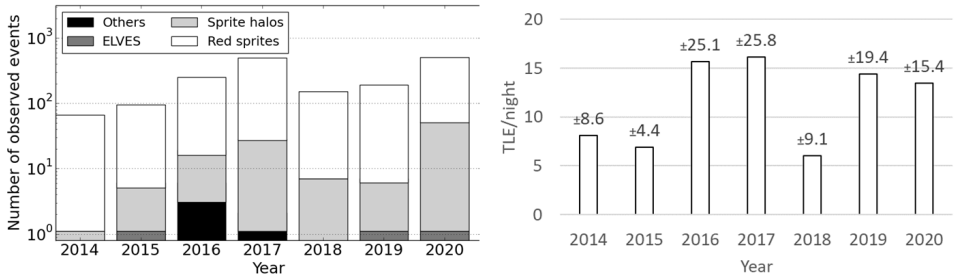
Fig. 6: Yearly summary of TLE records from Baja in the period 2014-2020. **Left:** number and types of observed events. Note the logarithmic scale. **Right:** average number of TLEs recorded in different years. The number of nights of successful observations was 9 in 2014, 13 in 2015, 15 in 2016, 29 in 2017, 24 in 2018, 13 in 2019, 34 in 2020. The standard deviations are written above each column.
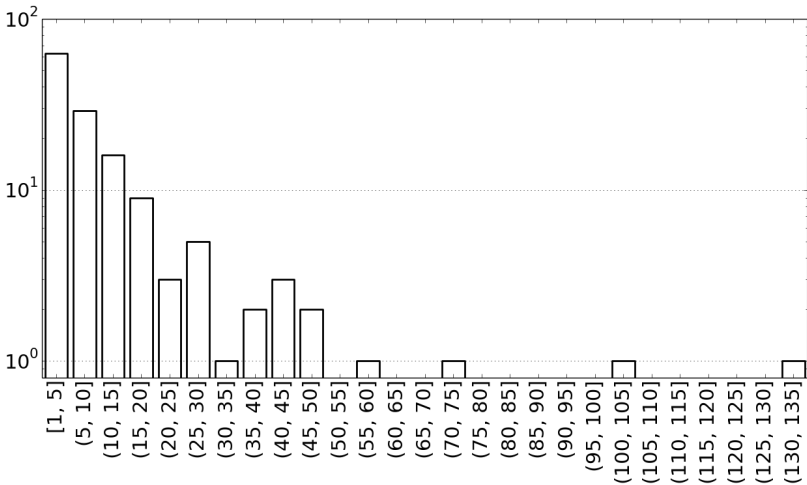

Fig. 7: Distribution of the number of TLEs that were observed on a single night from Baja in the period 2014-2020. Note the logarithmic scale.

Indeed, these statistics can be biased by exceptionally TLE-active thunderstorms which can produce an outstanding number of events on a single night. The distribution of events observed on a night (Fig. 7) clearly indicates this. In the considered years, the number of events observed on a single night was above 100 two times: 102 events were recorded on Sept 5, 2016, and 132 events were recorded on Aug 10, 2017. The histogram shown in Fig. 7 well mirrors the power law found for the number of events produced by lightning activity in a single thunderstorm in Europe (Arnone et al., 2020).
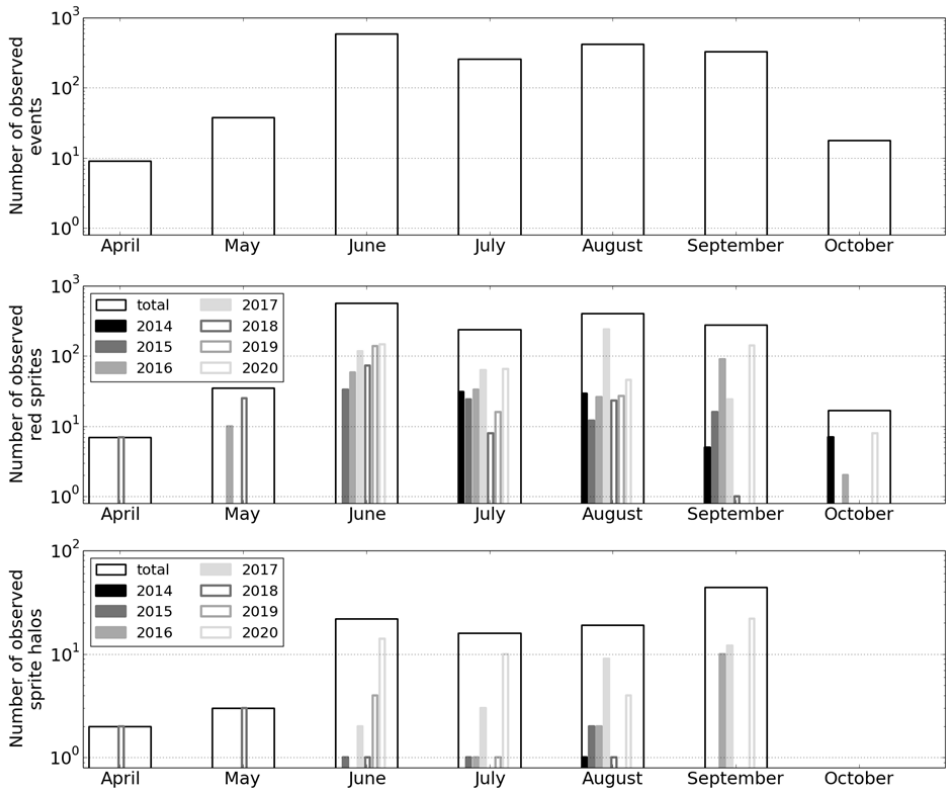

Fig. 8: Monthly number of TLEs observed from Baja in the period 2014-2020. **Upper panel:** total number of events. **Middle panel:** red sprites. **Lower panel:** sprite halos.

Observations were made in months from June to September almost in each year between 2014 and 2020, so comparing the number of observed TLEs in these months is meaningful (Fig 8). It can be seen that the most TLEs were observed in June and sprite occurrences dominate in this month. The outstanding number in August is only due to the exceptionally high number of events that were observed in 2017.
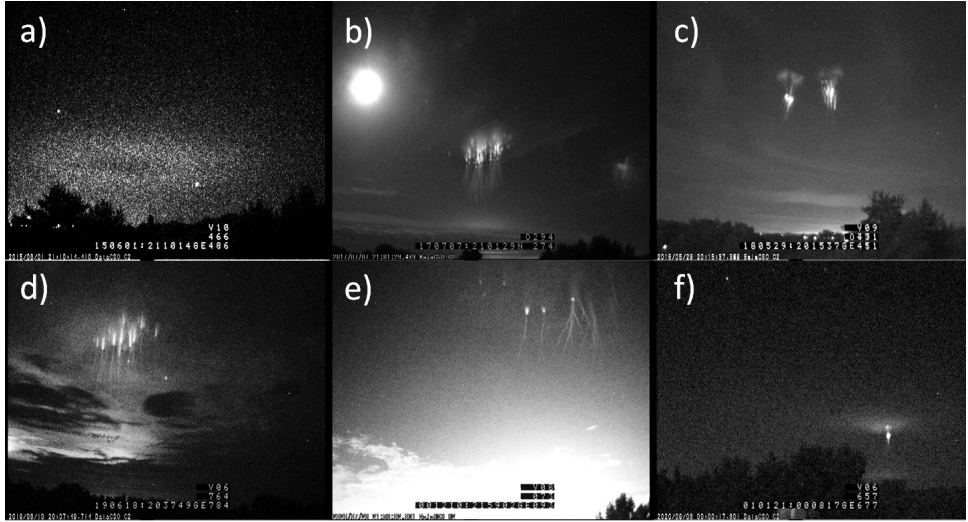
Fig. 9: Examples of TLEs observed from Baja. **a)** ELVES, Jun 1, 2015, 21:10 UTC, **b)** sprite cluster and the Moon, Jul 7, 2017, 21:01 UTC, **c)** carrot sprites, May 29, 2018, 20:15 UTC, **d)** sprite cluster close to Baja, Jun 18, 2019, 20:37 UTC, also see Fig. 4, **e)** very short column sprites with bright tendrils, Jul 26, 2020, 21:59 UTC, note the week number rollover error in the time stamp **f)** carrot sprite and sprite halo, Sep 6, 2020, 00:08 UTC, note the week number rollover error in the time stamp.

The middle and lower panels in Fig. 8 also reveal that the number of observed sprite halos does not have an obvious peak in any month of the observation period. Again, the outstanding number in September appears because of the great number of events detected in 2020. This difference between the observed numbers of these TLE types suggests that there may be a change in the characteristics of lightning strokes as autumn follows summer (Rakov & Uman, 2007, ch. 2.8, ch. 8), and the center of the lightning activity tends to move to the south (Arnone et al., 2020; Kotroni & Lagouvardos, 2016). Figure 9 shows examples of TLEs recorded in the considered years.

Summary

The second observation site in Hungary in support of organized scientific research on TLEs has been set up in the Astronomical Observatory in Baja in 2014. Since the installation up to 2020, 1655 TLEs were recorded above the covered area in Europe. The vast majority of the captured events are sprites but several sprite halos (106) were captured, too. Only 3 ELVES were detected unambiguously. Both the total number of recorded events and the average number of events captured during a night varies significantly from year to year. Uneven availability of observers, strongly varying local viewing conditions, and actual variation of TLE-producing potential of thunderstorms contribute to this variation. According to the experience, nevertheless, most sprites were captured in June while the greatest number of sprite halos have been detected from Baja so far in September.

Acknowledgements

References

AllMetSat (2021). Retrieved November 30, 2021, from https://hu.allmetsat.com/kepek/sat24_europe_ir.php

Arnone, E., Bór, J., Chanrion, O. et al. (2020). Climatology of Transient Luminous Events and Lightning Observed Above Europe and the Mediterranean Sea. *Surveys in Geophysics, 41*, 167–199, https://doi.org/10.1007/s10712-019-09573-5

BlitzOrtung (2021). Retrieved November 30, 2021, from https://www.blitzortung.org

Bór, J., Sátori G., & Betz H.D. (2009). Observation of TLEs in Central Europe from Hungary Supported by LINET. *AIP Conference Proceedings, 1118*(73), https://doi.org/10.1063/1.3137716

Bór, J. (2013). Optically perceptible characteristics of sprites observed in Central Europe in 2007–2009. *Journal of Atmospheric and Solar-Terrestrial Physics, 92*, 151-177, https://doi.org/10.1016/j.jastp.2012.10.008

Bór, J., Zelkó, Z., Hegedüs, T., Jäger, Z., Mlynarczyk, J., Popek, M., & Betz, H. D. (2018). On the series of +CG lightning strokes in dancing sprite events. *Journal of Geophysical Research: Atmospheres, 123*, 11,030–11,047, https://doi.org/10.1029/2017JD028251

ESTOFEX (2021). Retrieved November 30, 2021, from https://www.estofex.org/

Gordillo-Vázquez, F.J., & Pérez-Invernón, F.J. (2021). A review of the impact of transient luminous events on the atmospheric chemistry: Past, present, and future. *Atmospheric Research, 252*, 105432, https://doi.org/10.1016/j.atmosres.2020.105432

Hegedüs, T., Szatmáry, K., & Vinkó, J. (1992). Light-curve and O-C Diagram Analysis of RZ Cassiopeiae. *Astrophysics and Space Science, 187*, 57-74., https://doi.org/10.1007/BF00642687

Hsu, R.-R., Su, H.-T., Chen, A. B.-C., & Kuo, C.-L. (2017). Selected results from the ISUAL/FORMOSAT2 mission. *Terrestrial, Atmospheric and Oceanic sciences journal, 28*, 525-544, https://doi.org/10.3319/TAO.2016.08.23.01

Ill, M. (1983). *Structure of the upper atmosphere as inferred from deceleration of satellites and on-board measurements* (translated from the Hungarian title: *A felsőlégkör szerkezete a műholdak fékeződése és fedélzeti mérések alapján)* [Doctoral dissertation, Hungarian Academy of Sciences] REAL-d. http://real-d.mtak.hu/1039/

Kotroni, V. & Lagouvardos, K. (2016). Lightning in the Mediterranean and its relation with sea-surface temperature. *Environmental Research Letters, 11*(3), 034006, https://doi.org/10.1088/1748-9326/11/3/034006

LightningMaps.org (2021). Retrieved November 30, 2021, from https://www.lightningmaps.org/

Meteologix (2021). Retrieved November 30, 2021, from https://meteologix.com/hu/lightning/europe

Mitnyan, T., Bódi, A., Szalai, T., Vinkó, J., Szatmáry, K., Borkovits, T., Bíró, B.I., Hegedüs, T., Vida, K., & Pál, A. (2018). The contact binary VW Cephei revisited: Surface activity and period variation. *Astronomy and Astrophysics, 612*, A91, 14 p., https://doi.org/10.1051/0004-6361/201731402

Neubert, T., Østgaard, N., Reglero, V. et al. (2019). The ASIM Mission on the International Space Station. *Space Science Reviews, 215*, 26, https://doi.org/10.1007/s11214-019-0592-z

Pasko, V.P., Yair, Y., & Kuo, C.L. (2012). Lightning Related Transient Luminous Events at High Altitude in the Earth's Atmosphere: Phenomenology, Mechanisms and Effects. *Space Science Reviews, 168*, 475–516, https://doi.org/10.1007/s11214-011-9813-9

Rakov, V.A. & Uman, M.A. (2007). *Lightning: Physics and Effects.* New York, USA: Cambridge University Press, ISBN 9781107268555

Saltikoff, E., Haase, G., Delobbe, L., Gaussiat, N., Martet, M., Idziorek, D., Leijnse, H., Novák, P., Lukach, M., & Stephan, K. (2019). OPERA the Radar Project. *Atmosphere, 10*(6), 320, https://doi.org/10.3390/atmos10060320

Siingh, D., Singh, R.P., Singh, A.K. et al. (2012). Discharges in the Stratosphere and Mesosphere. *Space Science Reviews, 169*, 73–121, https://doi.org/10.1007/s11214-012-9906-0

Singh, A.K., Siingh, D., Singh, R.P., & Mishra, S. (2011). Electrodynamical Coupling of Earth's Atmosphere and Ionosphere: An Overview. *International Journal of Geophysics, 2011*, 971302, https://doi.org/10.1155/2011/971302

Schmetz, J., Tjemkes, S.A., Gube, M., & van de Berg, L. (1997). Monitoring deep convection and convective overshooting with METEOSAT. *Advances in Space Research, 19*(3), 433-441, https://doi.org/10.1016/S0273-1177(97)00051-3

Soula, S., Defer, E., Füllekrug, M., van der Velde, O., Montanya, J., Bousquet, O., Mlynarczyk, J., Coquillat, S., Pinty, J.-P., Rison, W., et al. (2015). Time and space correlation between sprites and their parent lightning flashes for a thunderstorm observed during the HyMeX campaign. *Journal of Geophysical Research: Atmospheres, 120*, 11552– 11574, https://doi.org/10.1002/2015JD023894

Surkov V.V. & Hayakawa M. (2020). Progress in the Study of Transient Luminous and Atmospheric Events: A Review. *Surveys in Geophysics, 41*, 1101-1142, https://doi.org/10.1007/s10712-020-09597-2

van der Velde, O. A., Montanyà, J., Soula, S., Pineda, N., & Mlynarczyk, J. (2014). Bidirectional leader development in sprite-producing positive cloud-to-ground flashes: Origins and characteristics of positive and negative leaders. *Journal of Geophysical Research: Atmospheres, 119*, 12755–12779, https://doi.org/10.1002/2013JD021291

Vinkó, J., Sárneczky, K., Takáts, K., Marion, G.H., Hegedüs, T., Bíró, I.B., Borkovits, T., Szegedi-Elek, E., Farkas, A., Klagyivik, P., Kiss, L.L., Kovács, T., Pál, A., Szakáts, R., Szalai, N., Szalai, T., Szatmáry, K., Szing, A., Vida, K., & Wheeler, J.C. (2012). Testing supernovae Ia distance measurement methods with SN 2011fe. *Astronomy & Astrophysics, 546*, A12, https://doi.org/10.1051/0004-6361/201220043

Wang, Y., Lu, G., Ma, M., Zhang, H., Fan, Y., Liu, G., Wan, Z., Wang, Y., Peng, K-M, Peng, C., Liu, F., Zhu, B., Ni, B., Gu, X., Chen, L., Yi, J., & Zhou, R (2019). Triangulation of red sprites observed above a mesoscale convective system in North China. *Earth and Planetary Physics, 3*, 111-125, http://doi.org/10.26464/epp2019015